

Optimizing information transmission in neural induction constrains cell surface contacts of ascidian embryos

Rossana Bettoni,^{1,2,3} Geneviève Dupont,^{1,3} Aleksandra M. Walczak,^{4,2,*} and Sophie de Buyl^{2,3,5,*}

¹*Unité de Chronobiologie Théorique, Faculté des Sciences, CP231, Université Libre de Bruxelles (ULB), Boulevard du Triomphe, Brussels, Belgium*

²*Applied Physics Research Group, Vrije Universiteit Brussel, Brussels, Belgium*

³*Interuniversity Institute of Bioinformatics in Brussels, ULB-VUB, La Plaine Campus, Brussels, Belgium*

⁴*Laboratoire de physique de l'École normale supérieure, CNRS, Paris Sciences et Lettres (PSL) University,*

Sorbonne Université, and Université de Paris, 75005 Paris, France.

⁵*Data Analytics Laboratory, Vrije Universiteit Brussel, Brussels, Belgium*

(Dated: October 22, 2024)

The onset of neural induction in the anterior ectoderm of ascidian embryos is regulated at the extracellular level by FGF signaling molecules, which control the acquisition of neural fate through the activation of the ERK pathway. Among the anterior ectoderm cells exposed to FGF, only a fraction will acquire neural fate. The selection of neural precursors depends on the quasi-invariant geometry of the embryo, which imposes upon each ectoderm cell a precise area of cell surface contact with underlying FGF-expressing (mesendoderm) cells. Here, we investigate information transmission between FGF and activated ERK and how this depends on the geometry of the system. Optimizing information transmission with the constraint that the total FGF-emitting surface area is restricted, as in the embryo, we find that the surface contacts with FGF that maximize information transmission are close to those observed experimentally. This information optimal solution is compatible with the anterior ectoderm cells having different areas of cell surface exposure to FGF, allowing the embryo to use cell surface areas as a regulatory mechanism for differentiating the outcome of cells that sense a constant FGF concentration.

I. INTRODUCTION

The information contained in the fertilized egg must be decoded by the developing embryo to transform the latter into an organized structure. This is achieved by combining mechanical interactions constrained by geometry and molecular signaling that is stochastic by nature, thereby limiting the transmission of the information. Optimization principles have been suggested to assess how close to the maximal possible transmitted information biological systems can operate [1–4]. Specifically, inspired by developmental regulation in early fly embryos, optimizing information between a spatially decaying input morphogen and downstream gene readouts has led to tiling solutions, where different genes make a readout in non-overlapping concentration domains [5, 6]. While the real regulatory networks in early fly development have proven more complex [3, 7], optimization of information transmission can contribute to explain the structure of cellular and molecular interactions that lead to the reproducibility of development and the emergence of a highly organized organism from a fertilized egg [4, 8]. Development is driven by the coordination and mutual dependence of genetically encoded signals, mechanical stress and geometry [9]. However while inference approaches have been proposed to link mechanical stresses and lineage structure in development [10, 11], optimizing infor-

mation transmission of signals has not been linked to embryo geometry. Here we use the well studied case of ascidian embryos to explore how information transmission of concentration-dependent signals constrains cell geometry in early embryos.

Ascidians exhibit a very simple and reproducible embryogenesis. Of particular interest is the fact that they develop, like nematodes, with an invariant cleavage pattern. This means that the positioning and timing of cell divisions are quasi-invariant between different individuals of the same species [12], leading to an extreme form of canalization [13]. Moreover, when the embryo consists of only 112-cells, the segregation of the major tissue-specific cell lineages (muscle, endoderm, nervous system etc) is almost completed. There is also no embryo growth or cell migration during early ascidian development. This type of embryogenesis makes it possible to follow each cell individually and trace the establishment of their fates, and therefore to address the question of cell fate segregation and the establishment of the body plan in a relatively simple context. Additionally, ascidian embryogenesis is extremely well documented [14]. Databases containing information about the geometry of the embryo, gene regulatory networks leading to the larval body plan and cell specific gene expression patterns are publicly available [15–20]. Recent works inferred cell pressures, membrane and line tensions at single-cell resolution reproducing the mechanical cell stresses observed during the early stages of ascidian gastrulation [10, 11]. Altogether these properties make ascidian embryogenesis an appealing toy

* Co-last authors

model to study cell fate decisions.

Contrary to the role that morphogen gradients have been shown to play during patterning of many other systems [21], in ascidians, short-range signals between contacting cells could explain all known early embryonic inductions [19]. In support of this, in our previous work we have shown that, during early neural induction at the 32-cell stage of development, measured areas of cell surface contact act as strong predictive determinants for differential cell fate specification [22, 23]. During neural induction, in response to an extracellular inductive signal (i.e., the fibroblast growth factor), specific cells in the embryo express the gene *Otx*. The process is mediated by the ERK signaling pathway (see section II for a detailed description of the neural induction process). Building on our previous studies, we analyze information transmission in the first step of neural induction: from the inducer FGF to the activation of ERK. We investigate whether the contact surfaces of four pairs of cells (a-line cells, Fig. 1(a)) involved in the process of neural induction are compatible with optimal information transmission between the inductive signal and ERK. More precisely, we ask if the probability distribution of the concentration of the inducer, i.e., the fibroblast growth factor (FGF), is read optimally by the cells through the portion of their surfaces that is in contact with this ligand.

To address this question we develop, in section III A, a stochastic model of the pathway involved in neural induction. This is a minimal version of the deterministic model we formulated in [22, 23]. In section III B, relying on the stochastic minimal model, we analyze information transmission in a single cell. More precisely, we investigate whether the information transmitted between FGF and the number of active ERK molecules (ERK*) depends on the geometrical configuration of the cell, i.e. on the surface of the cell in contact with FGF. In section III C, we investigate how the geometry of the system influences information transmission in the multi-cellular context. In particular, we consider the case in which all the cells are identical, except for their surface contacts with FGF. We perform this analysis in the presence of an external constraint which limits the total area of the cell surface contacts with FGF. To formulate this constraint problem, we first consider two cells and then we generalize the computation to the four-cell case. Finally, in section III D we turn to the case relevant for ascidian embryos and consider four cells with different total surfaces. We compute the areas of the cell surface contacts with FGF that maximize information transmission and compare them with the experimental measurements.

II. NEURAL INDUCTION IN THE ASCIDIAN EMBRYO

In ascidians, neural induction in anterior ectoderm cells is the first step of a complex process of cell fate specification that will generate the anterior-most part

of the larval central nervous system together with anterior placode-like structures [24, 25]. It takes place at the 32-cell stage of embryonic development (schematized in Fig. 1(a)), during a single cell cycle of about 30 minutes [23]. The embryo exhibits left-right symmetry and is divided into animal and vegetal hemispheres. The animal hemisphere will eventually give rise to mostly ectodermal tissues, the epidermis and part of the nervous system. The vegetal hemisphere generates mostly mesendoderm fates, the endoderm and mesoderm tissues including notochord and muscle as well as posterior central nervous system [19].

During neural induction, 2 out of 8 anterior ectoderm cells (a-line cells, shown in magenta, green, blue and dark gray in Fig. 1(a)) transcriptionally activate the neural marker *Otx* [23, 26]. The signaling pathway that controls the expression of *Otx* is complex, involving a large number of reactions [22, 27]. A simplified scheme of the pathway is shown in Fig. 1(b)). The process is initiated at the extracellular level by two signaling molecules: FGF and ephrin. FGF binding to its receptors R on the cell membrane activates the ERK signaling pathway which in turn induces the expression of *Otx*. At the same time, ephrin binding to its receptors Q on the cell membrane attenuates the activation of the ERK pathway thereby reducing the level of *Otx* expression. The activation of ERK (and therefore the expression of *Otx*) is also inhibited by ephrin-independent RasGAPs molecules (indicated as RasGAPs in Fig. 1(b)).

All the a-line cells are assumed to perceive the same concentration of FGF, produced by the underlying mesendoderm cells (shown in yellow in Fig. 1(a)) [23]. At the same time, the a-line cells are also in contact with ephrin, produced by all ectoderm cells. Despite the observation that all a-line cells are competent for neural induction and all of them are in contact with FGF, only the a6.5 pair of cells will undergo neural induction. Selection of neural precursors is controlled by the geometry of ectoderm cells, which dictates their contact surface areas with their FGF- and ephrin-expressing neighbors [22, 23].

III. RESULTS

A. Stochastic minimal model of ERK activation during neural induction

In our previous work [22, 23] we developed a computational model to describe the regulation of *Otx* expression by the FGF- and ephrin-regulated ERK pathway during ascidian neural induction. The model allowed us to show that differences in the surface contacts with FGF and ephrin are sufficient to control the process of neural induction at this stage in the embryo.

To address the question of information transmission, we develop a stochastic model of the pathway, reducing our previously developed model [22] to facilitate the derivation of analytical results and improve interpretability.

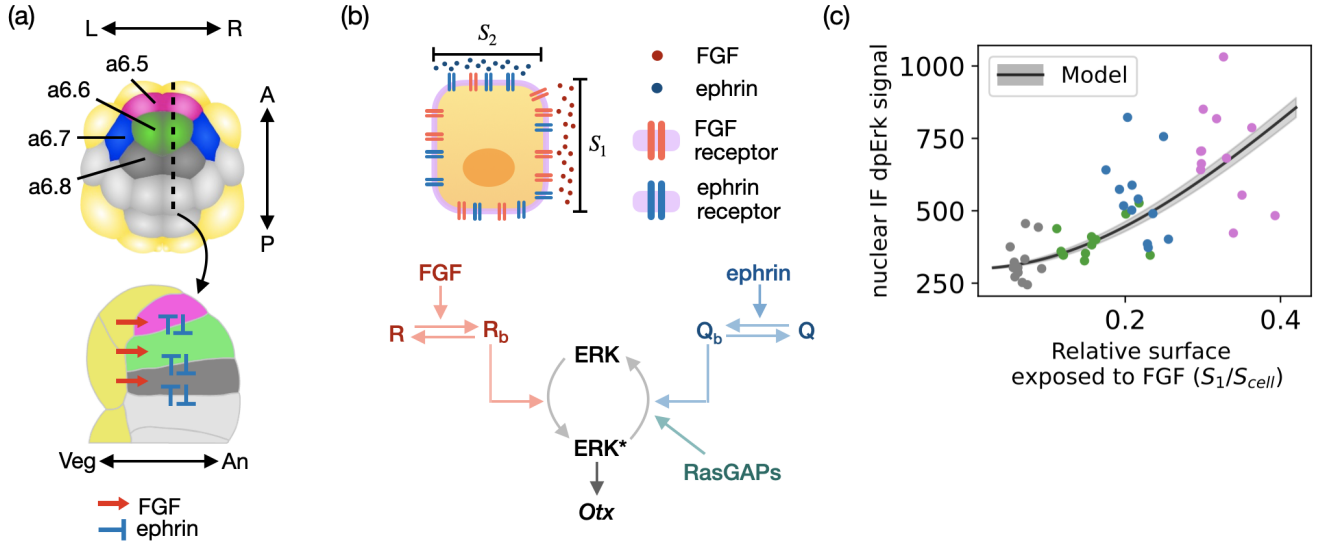


FIG. 1. (a) Cartoon of the 32-cell stage ascidian embryo. View of the animal side of the embryo (top). Anterior ectoderm cells (a-line cells), which can become neural, are indicated in different colors: a6.5 cells in magenta, a6.6 cells in green, a6.7 cells in blue, and a6.8 cells in dark gray. Mesendoderm cells are shown in yellow and posterior ectoderm cells (b-line cells) in light gray. The black dotted line is used for the sagittal section of the embryo shown at the bottom. FGF and ephrin signals are represented by red and blue arrows, respectively. The anterior-posterior (A-P), left-right (L-R) and vegetal-animal (Veg-An) axis of the embryo are indicated by double-sided arrows. The total cell surface areas of the different a-line cells are: $S_{\text{cell}}^{a6.5} = 6837 \pm 248 \mu\text{m}^2$, $S_{\text{cell}}^{a6.6} = 8268 \pm 172 \mu\text{m}^2$, $S_{\text{cell}}^{a6.7} = 7331 \pm 310 \mu\text{m}^2$, $S_{\text{cell}}^{a6.8} = 8646 \pm 135 \mu\text{m}^2$. Figure adapted from [23]. (b) Cartoon of the pathway leading to neural induction. The process is initiated at the extracellular level by the binding of FGF and ephrin to their receptors (R and Q , respectively) present on the cell membrane. The areas of the cell surface exposed to FGF and ephrin ligands are denoted by S_1 and S_2 . For simplicity the membrane bound ephrin ligands are not shown attached to the membrane of the emitting cell. Bound FGF receptors (R_b) induce the double phosphorylation of ERK. The active form of ERK (dpERK) is indicated in the scheme as ERK*. Bound ephrin receptors (Q_b) favor the de-activation of ERK*, which is also promoted by ephrin-independent RasGAPs molecules (indicated as RasGAPs in the scheme). ERK* induces the expression of the neural marker *Otx*. (c) Nuclear dpERK immunofluorescence (IF) signals measured experimentally in individual a-line cells as a function of the relative area of cell surface contact with FGF-expressing cells (S_1/S_{cell}). Experimental data obtained in the different cell types are shown with dots of different colors: a6.8 cells are shown in gray, a6.6 cells in green, a6.7 cells in blue, and a6.5 cells in magenta. The experimental data are compared with the model predictions (black line). The shaded region represents the noise in the level of ERK* fluorescence predicted by the model using the Langevin approach. The model predictions are obtained as described in section III A, V A and V B, with $c = 5$. The parameter values used to reproduce the experimental data are listed in Table I. $A = 8000$, $B = 280$, see section V B.

ity. The model consists of three stochastic differential equations describing the temporal evolution of the number of bound FGF receptors R_b , the number of bound ephrin receptors Q_b and the number of active (i.e., doubly phosphorylated) ERK molecules (E^*):

$$\dot{R}_b = k_{d+}c(R - R_b) - k_{d-}R_b + \xi_R; \quad (1)$$

$$\dot{Q}_b = k_{e+}e(Q - Q_b) - k_{e-}Q_b + \xi_Q; \quad (2)$$

$$\begin{aligned} \dot{E}^* = & V_s \frac{R_b^2}{R_b^2 + K_s^2} (E_T - E^*) \\ & - \left(V_{rg} \frac{Q_b}{Q_b + K_{rg}} + k \right) E^* + \xi_E. \end{aligned} \quad (3)$$

We consider relative values of FGF ($c = [FGF]/[FGF]_0$) and ephrin ($e = [\text{ephrin}]/[\text{ephrin}]_0$) concentrations, where

$[FGF]_0$ and $[\text{ephrin}]_0$ are baseline values of FGF and ephrin concentrations ($\simeq 0.1 \text{ nM}$). R and Q are the number of FGF and ephrin receptors exposed to FGF or ephrin in a cell. k_{d-} and k_{e-} are the unbinding rate constants of FGF and ephrin to their receptor. k_{d+} and k_{e+} are the binding rate constants of FGF and ephrin to their receptor multiplied by the baseline values $[FGF]_0$ and $[\text{ephrin}]_0$, respectively. E_T is the total number of ERK molecules present inside the cell. V_s and V_{rg} are the maximum rates of ERK activation and deactivation, K_s and K_{rg} are the half saturation constants for R_b and Q_b . The parameter k is a deactivation rate constant modeling the presence of ephrin-independent RasGAP activity [23]. ξ_R , ξ_Q and ξ_E denote white noise with zero mean and amplitudes A_R , A_Q and A_E given by Eqns. (23), (26) and (27) (see section V A). All parameter values are given in Table I.

Similarly to our previous model, we make two key as-

sumptions [23]. First, we assume that the density of FGF and ephrin receptors on the membrane of the cell is uniform. This implies that the number of receptors exposed to FGF (R) or ephrin (Q) in a cell is proportional to the fraction of the cell surface area exposed to FGF (S_1) or to ephrin (S_2):

$$R = R_T \frac{S_1}{S_{\text{cell}}}; \quad Q = Q_T \frac{S_2}{S_{\text{cell}}}; \quad (4)$$

where R_T and Q_T are the total number of FGF and ephrin receptors present on a cell and S_{cell} is the total surface of the cell. Second, we consider that all the reactions reach steady-state fast compared to the time-scale of the process (which occurs over 30 minutes). This is supported by the observation that the ERK pattern (a6.5>a6.7>a6.6>a6.8) appears to be established rather quickly, short after these cells form. This assumption allows us solve Eq.(1)-(3) for the steady state number of active ERK molecules (\bar{E}^*).

Additionally, at the 32-cell stage S_1 and S_2 are related through the empirical relation [23]:

$$S_2 = -1.13S_1 + 0.91S_{\text{cell}}. \quad (5)$$

Therefore we can compute the number of active ERK molecules as a function of only the surface of the cell exposed to FGF. We assume that all the a-line cells have the same number of receptors $R_T = Q_T = 2000$ and perceive the same extracellular concentrations of FGF and ephrin as in our previous work [22, 23]. We also neglect any diffusion of FGF and ephrin ligands beyond the boundaries of the cell contacts. As a result, the different levels of ERK* predicted by the model in the four a-line cells are a consequence of the different cell surface contacts with FGF and ephrin.

In Fig. 1(c) the experimental measurements of dpERK immunofluorescence (colored dots) obtained in the different a-line cells are compared with the level of ERK* fluorescence predicted with the model (black line) using the parameter values listed in table I. The level of ERK* fluorescence (and similarly the noise, shown in gray in the scheme) can be computed from the number of active ERK molecules, as described in section V B. Despite its simplicity, the model successfully reproduces the experimental data obtained in wild type and ephrin-inhibited embryos (see Fig. 1(c) and S1). The experimental data in both figures 1(c) and S1(c) are significantly more spread than the model predictions. As well as intrinsic noise, it is likely that cell to cell variability and experimental measurement noise contribute to the dispersion of the experimental data.

B. Single cell case: the information transmitted between FGF and ERK* depends on the geometry of the cell

To assess the influence of the geometry of the system on information transmission, we first analyze the case

in which a single cell is exposed to the extracellular ligands FGF and ephrin through the surfaces S_1 and S_2 , as schematized in Fig. 2(a). In response to the concentrations of FGF and ephrin, a given number of ERK molecules is activated in the cell (E^*). The mutual information transmitted between the input (c) and the output (E^*) can be computed as [28]:

$$I(c; E^*) = - \int P(E^*) \log_2(P(E^*)) dE^* + \int P(c) dc \int P(E^*|c) \log_2(P(E^*|c)) dE^*. \quad (6)$$

The input ($P(c)$), output ($P(E^*)$) and conditional ($P(E^*|c)$) distributions are schematized in Fig. 2(b). Since c cannot take negative values, we assume $P(c)$ to be a log-normal distribution centered around $c = \mu_c$ with variance σ_c^2 :

$$P(c) = \frac{1}{c\sigma\sqrt{2\pi}} \exp\left(-\frac{(\ln(c) - \mu)^2}{\sigma^2}\right); \quad (7)$$

where:

$$\mu = \ln\left(\frac{\mu_c^2}{\sqrt{\mu_c^2 + \sigma_c^2}}\right); \quad \sigma^2 = \ln\left(1 + \frac{\sigma_c^2}{\mu_c^2}\right). \quad (8)$$

In line with the assumption that there is no gradient of FGF, and that all the a-line cells perceive nearly the same concentration of FGF, we consider the input distribution to be very narrow ($\sigma_c = 1$ compared to the normalized binding constant of the FGF receptors $K_d = k_{d-}/k_{d+} = 60$, which corresponds to 6 nM), see Fig. 2(b) for a schematic representation. In the absence of more information, we assume the conditional distribution $P(E^*|c)$ to be a Gaussian centered around $E^* = \bar{E}^*(c)$ with variance $\sigma_e^2(c)$:

$$P(E^*|c) = \mathcal{G}(E^*, \bar{E}^*(c), \sigma_e^2(c)); \quad (9)$$

where $\bar{E}^*(c)$ is computed solving Eq.(1)-(3), at steady state and $\sigma_e^2(c)$ is obtained using the Langevin approach as described in section V A. Finally, the output distribution $P(E^*)$ can be computed directly from the input and conditional distributions as:

$$P(E^*) = \int P(E^*|c)P(c) dc. \quad (10)$$

Therefore, the amount of transmitted information $I(c; E^*)$ is determined once the input $P(c)$ and conditional $P(E^*|c)$ distributions are specified. Mutual information depends on the geometrical configuration of the cell (on S_1 and S_2) since both the mean $\bar{E}^*(c)$ and the variance $\sigma_e^2(c)$ of the conditional distribution $P(E^*|c)$ are functions of the surface areas S_1 and S_2 . At this stage in the embryo, S_2 can be computed from the value of S_1 through phenomenological Eq.(5) [23]. We can therefore study the dependence on the transmitted information solely as a function of S_1 .

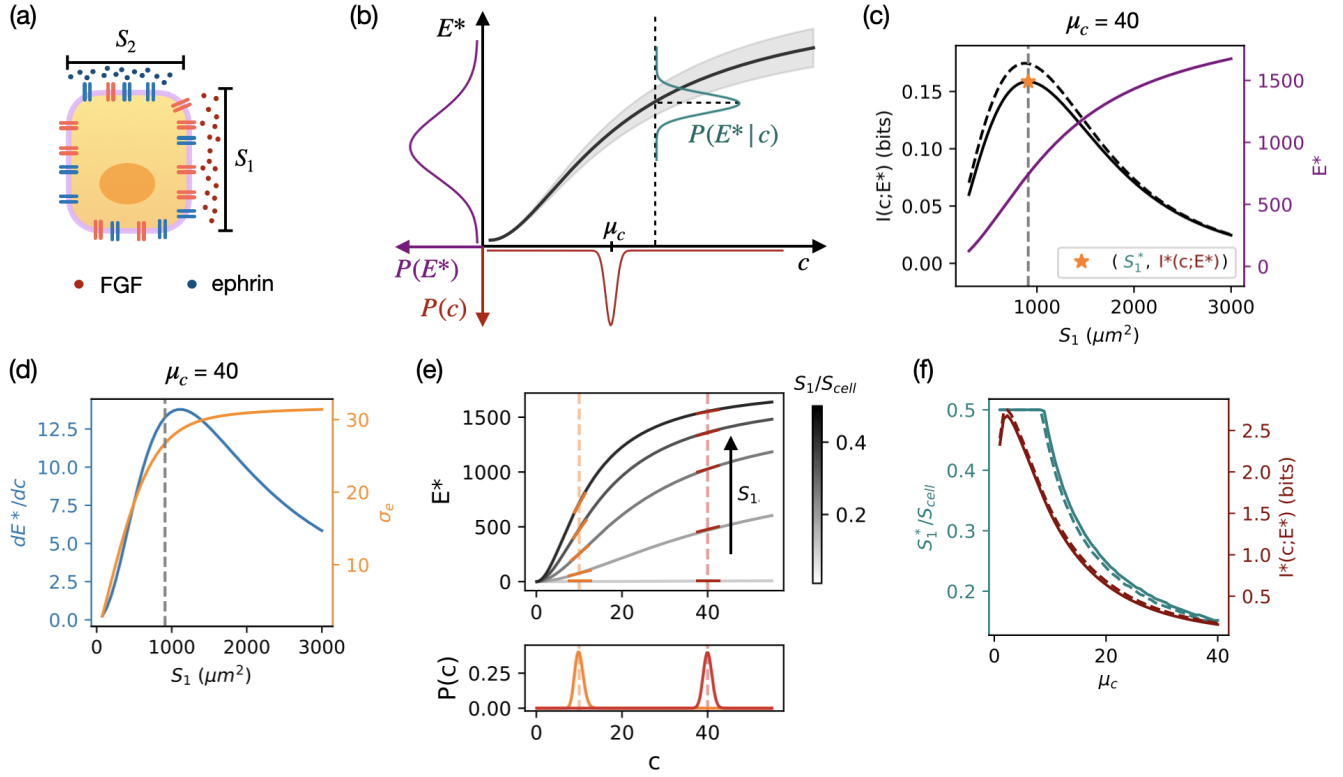


FIG. 2. (a) The single cell case. S_1 and S_2 are the areas of cell surface exposed to FGF and ephrin. The value of S_1 is constrained to be at most equal to $S_{\text{cell}}/2$, with S_{cell} being the total surface of the cell. The value of S_2 is computed from the value of S_1 using relation Eq.(5). (b) Scheme representing the input $P(c)$, conditional $P(E^*|c)$ and output $P(E^*)$ distributions. The distribution of the input $P(c)$ is a log-normal distribution centered around μ_c . The conditional distribution $P(E^*|c)$ is a Gaussian centered around $\bar{E}^*(c)$, with variance $\sigma_e^2(c)$. $\bar{E}^*(c)$ is the number of active ERK molecules in the cell and is computed with our model as described in section III A. $\sigma_e(c)$ is the noise in the number of ERK* molecules and is computed using the Langevin approach as described in section V A. (c) Information transmitted between the input c and the output E^* as a function of S_1 in the presence of ephrin (solid line) and in the absence of ephrin (dashed line). The maximal information (indicated as $I^*(c; E^*)$) is transmitted for $S_1 \simeq 910 \mu\text{m}^2$ (indicated with a star). In purple is represented the function $E^*(S_1)$ for $\mu_c = 40$. (d) The plot shows the steepness $\frac{d\bar{E}^*}{dc}|_{\mu_c}$ (in blue) and the noise $\sigma_e(c = \mu_c)$ (in orange) of the input-output relation $\bar{E}^*(c)$ as a function of S_1 . The curves are obtained with $\mu_c = 40$. The vertical gray line represents the value of S_1 for which the information transmitted $I(c; E^*)$ is maximal. (e) The main plot shows how the relation between \bar{E}^* and c varies depending on the value of S_1 . The value of S_2 is computed from the value of S_1 through Eq.(5). The lower plot shows the input distribution $P(c)$ centered at $\mu_c = 10$ (in orange) and at $\mu_c = 40$ (in red). The steepness of the curves close to $c = 10$ and $c = 40$ are shown in orange and red, respectively. (f) Maximal amount of information $I^*(c; E^*)$ (red curves) as a function of the position μ_c of the input distribution and the optimal value of S_1 (i.e. the value for which information transmission is maximal, green curves) as a function of μ_c , in the presence (solid lines) and absence (dashed lines) of ephrin. Panels (c), (d) (e) and (f) are obtained assuming: $S_{\text{cell}} = 6000 \mu\text{m}^2$, $\sigma_c = 1$.

We directly compute the mutual information $I(c; E^*)$ for increasing values of S_1 (Fig. 2(c)), for $\mu_c = 40$ which corresponds to 4 nM, and parameters given in table I. The curve obtained in the presence of ephrin (which is the physiological case, shown with a solid line in Fig. 2(c)) is compared with the curve obtained in the absence of ephrin (shown as a dashed line in Fig. 2(c)). Both curves have a maximum at intermediate values of S_1 ($\simeq 910 \mu\text{m}^2$). This may seem counter-intuitive since one could expect the maximum of information transmission to occur at the largest possible value of S_1 , when the highest number of ERK molecules can be activated.

The optimum cell surface area results from assuming a narrow input distribution $P(c)$, which limits the concentration range of the input-output relation in which information is transmitted to the narrow range defined by $c \simeq \mu_c$. More precisely, the amount of transmitted information $I(c; E^*)$ is determined by the steepness $d\bar{E}^*/dc(c)$ and the noise $\sigma_e(c)$ of the input-output relation close to $c = \mu_c$. The steepness of the curve determines how many different levels of ERK* can be distinguished by varying the input c , hence a higher steepness corresponds to a larger amount of transmitted information. The noise instead limits the ability to distinguish different levels of

the output and therefore higher levels of noise correspond to a lower amount of transmitted information.

When the input distribution is centered around $\mu_c = 40$ as in Fig.2(c), the steepness of the input-output relation has a peak for intermediate values of S_1 , while the noise monotonically increases with S_1 (see Fig. 2(d)). The optimal trade-off between maximizing the steepness and minimizing the noise is achieved by the surface area S_1^* (vertical gray line in Fig. 2(d)) at which the transmitted information is maximal.

The dependence of the steepness $d\bar{E}^*/dc(c)$ (compare orange and red bars in Fig. 2(e)) and noise $\sigma_e(c)$ (not shown) on S_1 are both a function of the mean input concentration μ_c , which results in different optimal surfaces S_1^* (green curves in Fig. 2(f)) and maximal amount of information $I^*(c; E^*)$ (red curves in Fig. 2(f)) for increasing values of μ_c . For small mean input concentrations, the maximal allowed cell surface area ($S_1 = S_{\text{cell}}/2$) is exposed to FGF. Information decreases with μ_c since the steepness of the input-output relation decreases (see Fig. 2(e)) and the noise increases (not shown).

The presence of ephrin (solid lines in Fig. 2(c) and (f)) only slightly reduces the amount of transmitted information (compare solid and dashed lines in Fig. 2 (c) and (f)) and has very little impact on the value of the optimal surface area S_1^* . The reduction of information in the presence of ephrin is most likely due to the fact that ephrin decreases both the number of active ERK molecules and the steepness of the input-output curve $d\bar{E}^*/dc(c)$.

C. Identical cell case: symmetry breaking is triggered by the constraint on the total surface

We now consider multiple cells exposed to FGF and ephrin. We first assume that all cells are identical, and differ only by the cell surface contacts with FGF and ephrin. All the other parameters of the model (including the total surface of the cells) have the same values in all the cells. We add an external constraint S_1^{tot} to take into account the limited area of FGF producing cells in the embryo (Fig. 3(a)).

We compute the information transmitted between the input c and the number of active ERK molecules E^* , generalizing the procedure in section III B as described in section V C. We investigate whether there is one (or more) geometrical configuration of the cells that maximizes information transmission and ask how the answer depends on the value of the constraint S_1^{tot} . The optimization procedure is described in section V D.

1. Two-cell case

To set up the framework we will first consider a two-cell system (Fig. 3(a)). The cells are exposed to FGF through the surfaces S_1^A and S_1^B and to ephrin through

the surfaces S_2^A and S_2^B (not marked in the cartoon). The number of ERK molecules activated in the two cells in response to the extracellular signals c and e are indicated by E_A^* and E_B^* . In each cell, the surface area exposed to ephrin ($S_2^{A,B}$) is computed from the corresponding value of S_1 using Eq.(5). As a consequence, the information $I(c; \{E_A^*, E_B^*\})$ transmitted between the input c and the outputs $\{E_A^*, E_B^*\}$ depends exclusively on the cell surface area in contact with FGF (S_1^A and S_1^B). The dependence of $I(c; \{E_A^*, E_B^*\})$ on S_1^A and S_1^B is shown in the heatmap in Fig. 3(b) for $\mu_c = 40$. At this value of μ_c , the input distribution $P(c)$ can be approximated with $\delta(c - \mu_c)$, since $\sigma_c \ll \mu_c$. The two cells therefore are basically independent and $I(c; \{E_A, E_B\}) = I(c; E_A) + I(c; E_B)$ (compare Fig. 3(b), (c) and (d) with Fig. S2(a), (b) and (c)). As a result, the globally optimum surface for the two cells is the same as the one obtained in the single cell case $S_1^{A*} = S_1^{B*} \simeq 910 \mu\text{m}^2$.

The presence of the external constraint S_1^{tot} imposes that $S_1^A + S_1^B = S_1^{\text{tot}}$. As a result, it restricts the possible values of S_1^A and S_1^B to straight lines defined by $S_1^B = S_1^{\text{tot}} - S_1^A$ (some of these lines are highlighted in the plot with different shades of gray, indicating different values of S_1^{tot}). The information $I(c; \{E_A^*, E_B^*\})$ computed along these lines is shown in the lower plot of Fig. 3(b) as a function of S_1^A . At low values of S_1^{tot} , the transmitted information has a single maximum (light gray curve in Fig. 3(b)). In this regime, information transmission is maximized when both cells expose the same area of cell surface to FGF ($S_1^{A*} = S_1^{B*} = S_1^{\text{tot}}/2$). At higher values of S_1^{tot} , information has two equivalent maxima, one for small S_1^A (and large S_1^B) and another one for large S_1^A (and small S_1^B) (dark gray curve in Fig. 3(b)). In this case, in order to maximize information transmission the two cells need to break their symmetry and expose different surfaces to FGF.

This is analyzed in more detail in Fig.3(c) and (d). The maximal amount of information $I^*(c; \{E_A^*, E_B^*\})$ computed for increasing values of the constraint S_1^{tot} is shown with a solid line in Fig. 3(c). The maximal information, transmitted when the cells expose the optimal surface areas to FGF, is compared to the information transmitted when the cells expose the same surface areas to FGF (I_{sym} , shown with a dashed line in Fig. 3(c)). The purple background highlights the values of S_1^{tot} for which the symmetry breaking favors information transmission. The optimal values of S_1^A are shown in Fig. 3(d) for increasing values of S_1^{tot} . For small S_1^{tot} , there is a single optimal value for S_1^A . As S_1^{tot} increases, one cell initially reaches the maximum allowed surface area exposed to FGF ($S_1 = S_{\text{cell}}/2$) set by the total cell area. At this point, the other cell increases its value of S_1 until it also hits the maximum allowed value $S_{\text{cell}}/2$ (Fig. 3(d)).

Since the two cells are independent, the symmetry breaking can be simply explained by the properties of the single cell curve (Fig. 2(c)). More precisely, it is the concavity of the single cell curve that determines which geometrical configuration of the cells maximizes information

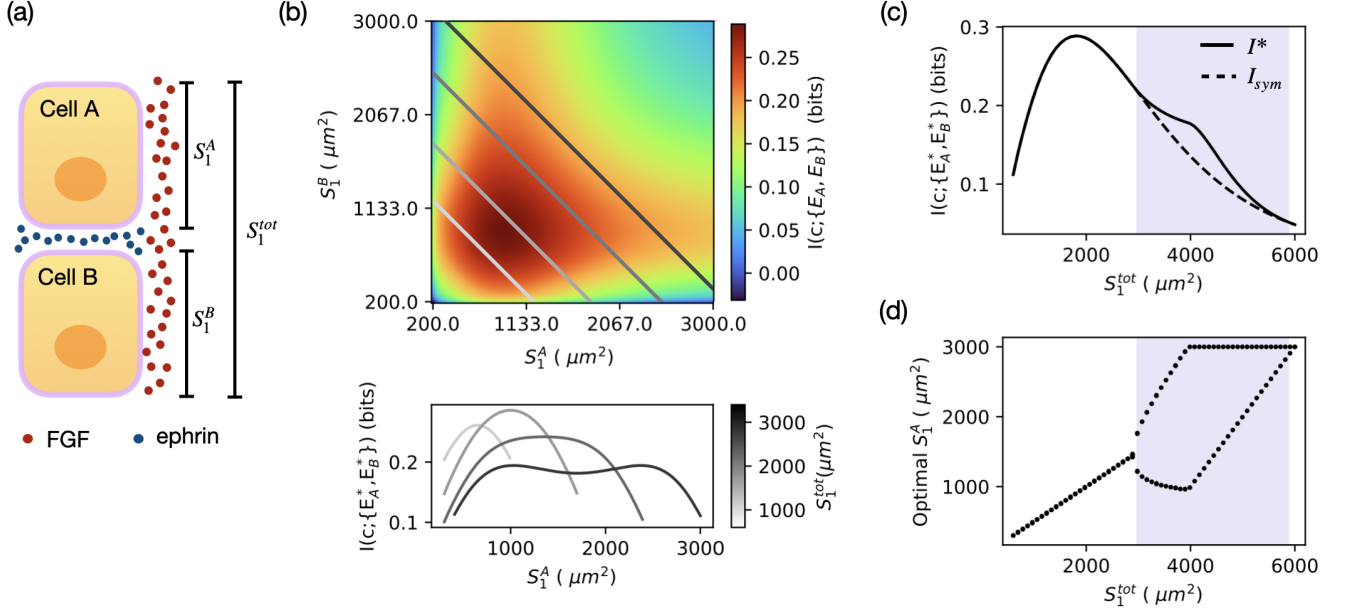


FIG. 3. (a) The two-cell case. S_1^A and S_1^B are the surface areas of the cells exposed to FGF. S_2^A and S_2^B (not shown in the cartoon) are the surface areas of the cells exposed to ephrin. In each cell, $S_2^{A,B}$ is computed from the corresponding value of $S_1^{A,B}$ using equation Eq.(5). The value of S_1 in each cell is constrained to be at most equal to $S_{\text{cell}}/2$, with S_{cell} being the total surface area of the cell. S_1^{tot} represents the total surface area where FGF is present. The presence of the constraint implies that $S_1^A + S_1^B = S_1^{\text{tot}}$. (b) The heatmap represents the information transmitted between the FGF input c and the ERK output $\{E_A^*, E_B^*\}$ as a function of the area of cell surfaces exposed to FGF (S_1^A and S_1^B). The presence of the constraint restricts the possible values of S_1^A and S_1^B to straight lines defined by $S_1^B = S_1^{\text{tot}} - S_1^A$. The straight lines colored with different shades of gray represent the accessible values of S_1^A and S_1^B for the values of S_1^{tot} used in the plot below. The plot below represents $I(c; \{E_A^*, E_B^*\})$ as a function of S_1^A for different values of the constraint S_1^{tot} (see colorbar). (c) Maximal information (I^*) transmitted between the FGF input c and the ERK output $\{E_A^*, E_B^*\}$ (solid line, obtained when the two cells expose the optimal surface areas to FGF) and the information transmitted when the two cells have the same surface areas exposed to FGF (I_{sym} , dashed line) as a function of S_1^{tot} . (d) Optimal values of S_1^A as a function of S_1^{tot} . The purple background highlights the regions of the plots where it is maximally informative for the two cells to expose different surface areas to FGF. Panels (b), (c) and (d) are obtained assuming $\mu_c = 40$, $\sigma_c = 1$, $S_{\text{cell}}^A = S_{\text{cell}}^B = 6000 \mu\text{m}^2$.

transmission. At low values of S_1^{tot} only the first part of the curve is accessible (see scheme in Fig. S2(d)). Since the curve in this region is concave, the information transmitted by two symmetric cells is larger than any other set of S_1^A and S_1^B that satisfies $S_1^A + S_1^B = S_1^{\text{tot}}$. As a result, the cells maximize information transmission when $S_1^A = S_1^B = S_1^{\text{tot}}/2$. The opposite occurs for large values of S_1^{tot} . In this case the accessible region the curve is convex (see scheme in Fig.S2(d)) and therefore the two cells maximize information transmission when $S_1^A \neq S_1^B$. The transition between these two regimes (i.e., the symmetry breaking) occurs at $S_1^{\text{tot}}/2 \simeq 1490 \mu\text{m}^2$ corresponding to the inflection point of the single cell curve.

We obtain qualitatively the same results in the absence of ephrin (see supplementary Fig. S3(a)). Both in the presence and in the absence of ephrin, the amount of transmitted information is quite low (less than 1 bit), but this is strongly dependent on the position μ_c of the input distribution, as shown in Fig. S3(b). Not only the amount of information, but also the values of S_1^{tot} for which the symmetry breaking occurs depend on μ_c (see

supplementary Fig. S3(b)).

The case in which the two cells have different total surfaces ($S_{\text{cell}}^A = 3000 \mu\text{m}^2$, $S_{\text{cell}}^B = 6000 \mu\text{m}^2$) is schematized in Fig. S4(a). The dependence of $I(c; \{E_A^*, E_B^*\})$ on S_1^A and S_1^B is shown in the heatmap in Fig. S4(b). As for the case in which the cells are identical, there is a single optimal value for the two cell surfaces in the absence of the constraint, with the difference that now the optimal values are different for the two cells ($S_1^{A*} \simeq 455 \mu\text{m}^2$, $S_1^{B*} \simeq 910 \mu\text{m}^2$). The transmitted information $I(c; \{E_A^*, E_B^*\})$ computed for different values of the constraint is shown in the lower plot of Fig. S4(b) as a function of S_1^A . As can be seen by comparing Fig.3(b) and Fig. S4(b), the asymmetry introduced in the total cell surfaces distorts the curves. In particular when S_1^{tot} is large (as for the dark gray curve), the two peaks in the curve are no longer equivalent. As a result, there is one single optimal geometrical configuration of the cells (with $S_1^{A*} < S_1^{B*}$, see Fig. S4(c)). Moreover, the optimal surface contacts with FGF (S_1^{A*} and S_1^{B*}), are always different, regardless of the value of S_1^{tot} see Fig. S4(c)).

2. Four-cell case

We now generalize the computation for the four-cell case, which is the condition that resembles what happens in the embryo during neural induction with four anterior animal cells (a6.5, a6.7, a6.6, a6.8) exhibiting different levels of ERK* in response to the extracellular FGF and ephrin signals (Fig. 4(a)). We consider four cells labeled A, B, C and D . The levels of ERK* in the cells are indicated by E_A^* , E_B^* , E_C^* and E_D^* . Computing S_2 from the value of S_1 with Eq.(5) results in the information $I(c; \{E_A^*, E_B^*, E_C^*, E_D^*\})$ depending only on the cell surface areas in contact with FGF (S_1^A , S_1^B , S_1^C and S_1^D). Similarly to the two-cell case, the presence of the constraint implies that $S_1^A + S_1^B + S_1^C + S_1^D = S_1^{\text{tot}}$.

We compute the maximal transmitted information $I^*(c; \{E_A^*, E_B^*, E_C^*, E_D^*\})$ (Fig. 4(b)) and the corresponding optimal surface areas (S_1^{A*} , S_1^{B*} , S_1^{C*} and S_1^{D*} , Fig. 4(c)) for increasing values of the constraint S_1^{tot} . As in the two-cell case, we find that the constraint S_1^{tot} controls the symmetry breaking in the cell surface areas in contact with FGF. More precisely, the value of S_1^{tot} determines whether the optimal geometrical configuration of the cells corresponds to four cells that expose the same surface area $S_1^{A*} = S_1^{B*} = S_1^{C*} = S_1^{D*} = S_1^{\text{tot}}/4$ to FGF (regions of Fig. 4(b) and (c) with white background) or to four cells that expose different surface areas to FGF (regions of Fig. 4(b) and (c) with purple and red backgrounds). The purple regions correspond to values of S_1^{tot} for which there are two optimal values for S_1^A . We also find regions (red backgrounds) with three optimal values for S_1^A . As for the two-cell case, the values of the constraint for which the symmetry breaking occurs, the maximal information transmitted $I^*(c; \{E_A^*, E_B^*, E_C^*, E_D^*\})$ and the optimal surface areas depend on the mean value of the FGF input distribution μ_c (not shown).

D. The contact surface areas measured experimentally are compatible with optimal information transmission

In this section we investigate whether the surface contacts of the a-line cells with FGF-expressing mesoderm cells in the embryo could be optimized for information transmission. We perform the same calculations as in the four-cell case described in the previous section, but now we consider that the total surface areas of the four cells (S_{cell}^A , S_{cell}^B , S_{cell}^C , S_{cell}^D) are equal to the ones measured experimentally in a6.5, a6.6, a6.7 and a6.8 cells. Similarly we consider the value of S_1^{tot} to be equal to the value measured experimentally.

We compute the optimal surface areas S_1^{A*} , S_1^{B*} , S_1^{C*} and S_1^{D*} in each embryo and compare them to the values of S_1 measured experimentally in the different a-line cells. As the optimal surfaces vary depending on the mean value of the input distribution μ_c (see Fig.4(d)),

we consider that the value of μ_c can be slightly different in different embryos. For each embryo we choose the value of μ_c that minimize the difference between the optimal and experimental data (highlighted with the vertical dashed line in Fig. 4(d)). The values of μ_c that match the experimental data ($\mu_c = 5.4 \pm 0.4$) are close to the value of [FGF] used to reproduce the experimental data in Fig1(c) ($c = 5$). The computed and measured distributions of S_1/S_{cell} are shown in Fig. 4(e). The optimal surface areas obtained by maximizing information transmission can be matched surprisingly well to those obtained experimentally. The optimal surfaces preserve the order of normalized cell surfaces (S_1/S_{cell}) observed experimentally (a6.5 > a6.7 > a6.6 > a6.8) in the vast majority of the embryos (23/25). The two exceptions (not shown in Fig.4(e)) are due to the fact that in these embryos cell a6.5 is larger than cell a6.7 ($S_{\text{cell}}^{a6.5} > S_{\text{cell}}^{a6.7}$). The amount of transmitted information is $\simeq 2.4 \pm 0.1$ bits, which is enough to unambiguously specify different levels of ERK* in the four cells, which would require $\log_2(4) = 2$ bits.

IV. DISCUSSION

Information transmission during ascidian neural induction depends on the geometry of the cells in the embryo, via the surface contacts with FGF-expressing cells. Here we investigated this dependence both in the single (as in section III B) and multiple (as in sections III C and III D) cell case. In the multicellular case, the presence of the external constraint S_1^{tot} plays a crucial role in determining the optimal geometrical configurations of the cells. In particular, the constraint determines whether the configuration that maximizes information transmission consists of cells that expose identical (or different) surface areas to extracellular FGF.

The contact surface areas of the a-line cells in the ascidian embryos at the 32-cell stage could be close to optimal for information transmission (see Fig. 4(e)). This is rather surprising since embryo and molecular configurations are expected to be under multiple selective pressures. Moreover, at the level of the whole developing embryo, the ERK pathway is used to specify a variety of distinct cell types [29, 30]. Any alterations to cell signaling or contacts will likely have an impact on subsequent patterning events. For these reasons, we would rather hypothesize that optimization of information transmission would be taking place at the level of the whole embryo patterning. Specifically, the quantity that may be optimized is the information transmitted between the morphogens in the egg and the expression levels of the genes needed to specify all the different cell fates.

The observed results may be further refined if we take into account other outputs regulated by the ERK pathway such as *Otx*. Such refinement has been observed for positional information in the context of gap genes in early *Drosophila* development, where each of the gap

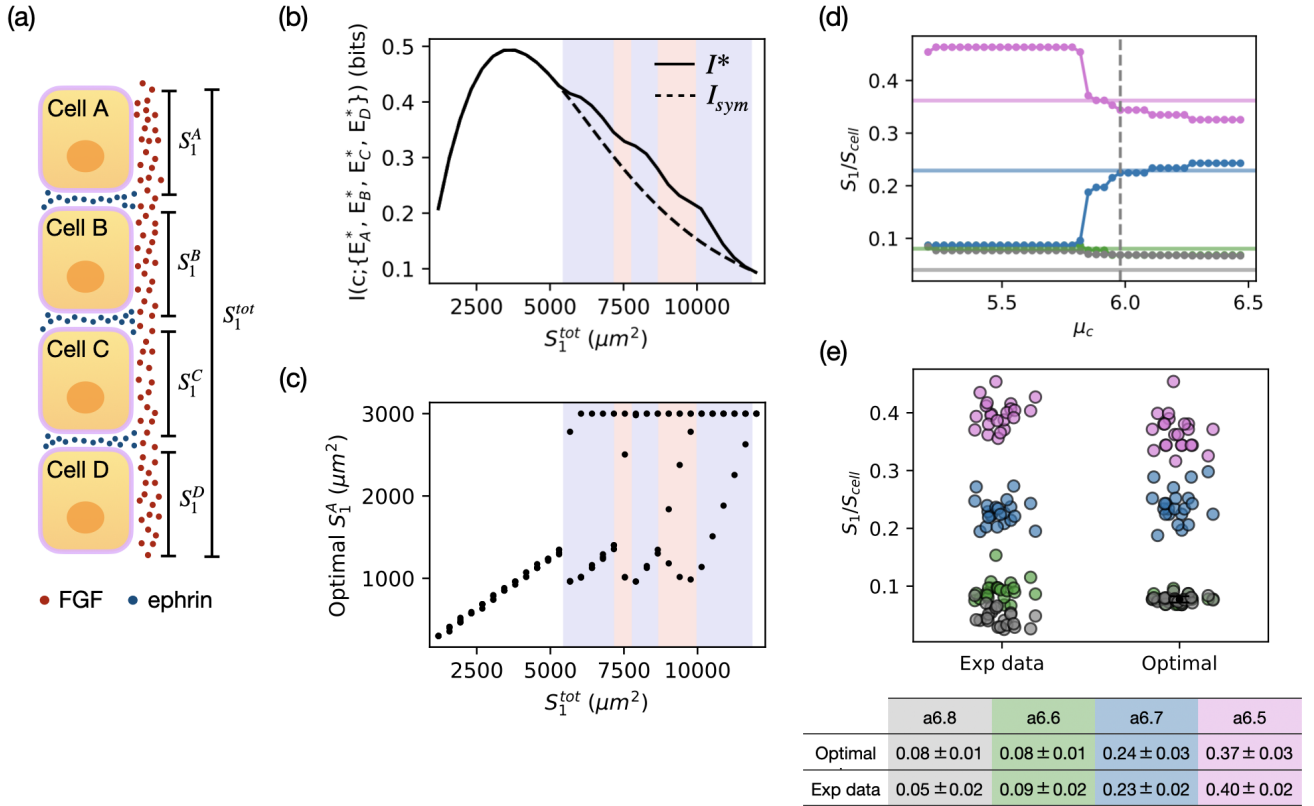


FIG. 4. (a) The four-cells case. We consider four cells (labeled A, B, C and D) exposed to FGF and ephrin. In each cell, the surface area exposed to ephrin (S_2 , not shown in the scheme) is computed from the corresponding value of S_1 using equation Eq.(5). We assume that the value of S_1 in each cell is constrained to be at most equal to $S_{\text{cell}}/2$ with S_{cell} being the total surface area of the cell. S_1^{tot} represents the total surface area where FGF is present. The presence of this constraint imposes that $S_1^A + S_1^B + S_1^C + S_1^D = S_1^{\text{tot}}$. (b) Maximal information (I^*) transmitted between c and $\{E_A^*, E_B^*, E_C^*, E_D^*\}$ (solid line, obtained when the cells expose the optimal surface areas to FGF) and the information transmitted when the four cells expose the same surface area to FGF (I_{sym} , dashed line) as a function of S_1^{tot} . (c) Optimal values of S_1^A as a function of S_1^{tot} . In the regions of the plot with purple and red backgrounds there are two or three optimal surface areas, respectively. These plots are obtained assuming $\mu_c = 40$, $\sigma_c = 1$, $S_{\text{cell}}^A = S_{\text{cell}}^B = S_{\text{cell}}^C = S_{\text{cell}}^D = 6000 \mu\text{m}^2$. (d) Optimal values of the surface areas exposed to FGF (S_1^{A*} in magenta, S_1^{B*} in green, S_1^{C*} in blue and S_1^{D*} in gray) as a function of the position μ_c of the input distribution. The optimal values are obtained maximizing information transmission in a single embryo using the values of S_1^{tot} , S_{cell}^A , S_{cell}^B , S_{cell}^C and S_{cell}^D measured experimentally. The horizontal lines represent the values of S_1 measured in a6.5 (magenta), a6.6 (green), a6.7 (blue) and a6.8 cells (gray) obtained in the same embryo. The vertical dashed line highlights the value of μ_c for which the difference between optimal and experimental values is minimal. (e) Comparison between the values of S_1/S_{cell} measured experimentally (on the left) and the closest matching optimal values of S_1/S_{cell} obtained by maximizing information transmission (on the right) in each embryo. The optimal values of S_1 are computed using the values of the total cell surface areas measured experimentally in the four a-line cells. The value of S_1^{tot} is also obtained from the experimental data. Each point represents a single cell. The points are colored depending on the cell type (a6.5 in magenta, a6.6 in green, a6.7 in blue and a6.8 in gray). The optimal values are compared with the ones measured experimentally in the table below the plot. For each cell type is computed the mean value of $S_1/S_{\text{cell}} \pm$ the standard deviation.

genes decreases the uncertainty in the readout of the Bcd gradient relative to the positioning of nuclei along the anterior-posterior axis [3].

Optimization of information transmission in neural induction can also be tackled from a different perspective, assuming the input of our system to be the different cell surface contacts with FGF-expressing cells (S_1) and not FGF concentration. Experimentally we have access to the distribution of the relative cell surface contacts

(S_1/S_{cell}). We could have optimized $I(S_1, E^*)$ and compared the optimal distribution of surface contacts with the one measured experimentally. The challenge of this approach consists in the computation of the optimal distribution $P(S_1^A, S_1^B, S_1^C, S_1^D)$. This problem, which is hard to solve analytically because of the presence of multiple inputs, could be addressed numerically by the use of the Blhaut-Arimoto algorithm [31]. We analyze the case of a single cell in appendix . As shown in Fig.6, the

results obtained by optimizing $P(S_1)$ are in qualitative agreement with the ones obtained in section III B, with the prediction of a single cell surface optimizing information transfer in the presence of a constraint on the area of the cell exposed to FGF.

Further refinement in understanding the interplay between geometry and signaling in ascidian development includes solving the problem of information transmission in realistic 3D geometries, including cellular tensions and divisions. Extending the approach of [11] to the 32-cell stage embryo and combining it with the signaling transmission considered here is an interesting, although difficult extension. Another important aspect of embryogenesis, that we did not address in this work, is its reproducibility across embryos. This could be tackled by adopting the approach described in [4].

The importance of the contact surface areas is not only limited to the establishment of the body plan. Despite genetic diversity different ascidian species show very similar early development, and in particular the geometric arrangement of the cells across different species is conserved [12, 14, 32]. Overall, relying on surfaces of contact for development might be a way of being robust under parameter and genetic changes.

In summary, optimizing information transmission in neural induction we find that the optimal configuration of the a-line cells is the one in which the cells expose different surfaces to FGF (Fig. 4(e)). This is the same as what occurs in real embryos in which the a-line cells expose different surface areas to FGF. The surface areas are used by the cells as a knob to tune the level of signal they receive, which is in turn translated into different activation levels of ERK, leading eventually to differential cell fate induction. This approach suggests that ascidian neural induction may be a consequence of the geometrical constraint imposed on the system.

V. METHODS

The model is implemented in Python. All the codes and the experimental data are available at: <https://github.com/rossanabettoni/Information-transmission-NI>.

A. Stochastic model of ERK activation

To compute the variance in the number of active ERK molecules we use the Langevin approach [2, 33]. We linearize equations (1)-(3) around steady-state and compute the response of the variables R_b, Q_b and E^* to the noise ξ_R, ξ_Q, ξ_E^* . The Langevin noise terms ξ_R, ξ_Q and ξ_E are defined by their statistical properties. They have zero mean:

$$\langle \xi_R(t) \rangle = \langle \xi_Q(t) \rangle = \langle \xi_E(t) \rangle = 0$$

and are uncorrelated in time:

$$\begin{aligned} \langle \xi_R(t) \xi_R(t') \rangle &= A_R \delta(t - t'); \\ \langle \xi_Q(t) \xi_Q(t') \rangle &= A_Q \delta(t - t'); \\ \langle \xi_E(t) \xi_E(t') \rangle &= A_E \delta(t - t'); \end{aligned} \quad (11)$$

where the noise amplitudes A_R, A_Q, A_E are given in Eqn 23, 26 and 27.

The evolution equations for small departures from steady-state are:

$$\delta \dot{R}_b = -(k_{d+}c + k_{d-})\delta R_b + \xi_R; \quad (12)$$

$$\delta \dot{Q}_b = -(k_{e+}e + k_{e-})\delta Q_b + \xi_Q; \quad (13)$$

$$\delta \dot{E}^* = \Gamma_R \delta R_b - \Gamma_Q \delta Q_b - \tau_E^{-1} \delta E^* + \xi_E; \quad (14)$$

where:

$$\Gamma_R = 2 V_S \frac{\bar{R}_b}{(\bar{R}_b^2 + K_S^2)^2} (E_T - \bar{E}^*);$$

$$\Gamma_Q = V_{rg} \frac{K_{rg}}{(\bar{Q}_b + K_{rg})^2} \bar{E}^*;$$

$$\tau_E^{-1} = V_s \frac{\bar{R}_b^2}{\bar{R}_b^2 + K_s^2} + V_{rg} \frac{\bar{Q}_b}{\bar{Q}_b + K_{rg}} + k.$$

The steady-state values for the number of bound FGF and ephrin receptors are given by:

$$\bar{R}_b = R \frac{c}{c + K_d}; \quad \bar{Q}_b = Q \frac{e}{e + K_e};$$

where $K_d = k_{d-}/k_{d+}$ and $K_e = k_{e-}/k_{e+}$.

Equations (12)-(14) can be solved introducing the Fourier transforms:

$$\delta R_b(t) = \int \frac{d\omega}{2\pi} e^{-i\omega t} \delta \tilde{R}_b(\omega);$$

$$\delta Q_b(t) = \int \frac{d\omega}{2\pi} e^{-i\omega t} \delta \tilde{Q}_b(\omega);$$

$$\delta E^*(t) = \int \frac{d\omega}{2\pi} e^{-i\omega t} \delta \tilde{E}^*(\omega).$$

Similarly, the Langevin noise terms can be written with the Fourier representation:

$$\xi(t) = \int \frac{d\omega}{2\pi} \tilde{\xi}(\omega).$$

Solving equation (12) for $\delta \tilde{R}_b$ we obtain :

$$\delta \tilde{R}_b(\omega) = \frac{\tilde{\xi}_R}{-i\omega + \tau_c^{-1}}; \quad (15)$$

Parameter	Definition	Value
$c = \frac{[\text{FGF}]}{[\text{FGF}]_0}$	Relative extracellular concentration of FGF, $[\text{FGF}]_0 \simeq 0.1$ nM	Variable
$e = \frac{[\text{eph}]}{[\text{eph}]_0}$	Relative extracellular concentration of ephrin, $[\text{eph}]_0 \simeq 0.1$ nM	5
E_T	Total number of ERK molecules	4000
k	ERK* de-activation constant	0.2 s^{-1}
k_{d-}	Unbinding rate constant of FGF to its receptor	6 s^{-1}
k_{d+}	Binding rate constant of FGF to its receptor multiplied by $[\text{FGF}]_0$	0.1 s^{-1}
k_{e-}	Unbinding rate constant of ephrin to its receptor	4 s^{-1}
k_{e+}	Binding rate constant of ephrin to its receptor multiplied by $[\text{eph}]_0$	0.1 s^{-1}
K_{rg}	Half saturation constant for Q_b	200
K_S	Half saturation constant for R_b	200
Q_T	Total number of ephrin receptors	2000
R_T	Total number of FGF receptors	2000
S_1	Surface exposed to FGF	Variable
S_2	Surface exposed to ephrin	Variable
S_{cell}	Total surface of one cell	$6000 \mu\text{m}^2$
V_S	Maximum rate of ERK activation	0.2 s^{-1}
V_{rg}	Maximum rate of ERK deactivation	0.08 s^{-1}

TABLE I. Default values of the parameters of the model.

where $\tau_c^{-1} = (k_{d+}c + k_{d-})$. Solving equation (13) for $\delta\tilde{Q}_b$ we obtain:

$$\delta\tilde{Q}_b(\omega) = \frac{\tilde{\xi}_Q}{-i\omega + \tau_e^{-1}}; \quad (16)$$

where $\tau_e^{-1} = (k_{e+}e + k_{e-})$. Finally, solving equation (14) we obtain:

$$\delta\tilde{E}^*(\omega) = \frac{\Gamma_R \delta\tilde{R}_b}{-i\omega + \tau_E^{-1}} - \frac{\Gamma_Q \delta\tilde{Q}_b}{-i\omega + \tau_E^{-1}} + \frac{\tilde{\xi}_E}{-i\omega + \tau_E^{-1}}. \quad (17)$$

The noise power spectral density of the protein copy number is:

$$S_E(\omega) = \langle \delta\tilde{E}^*(\omega) \delta\tilde{E}^{*\dagger}(\omega) \rangle; \quad (18)$$

where the \dagger indicates the complex conjugate.

$$S_E(\omega) = \frac{\Gamma_R^2 \langle \delta\tilde{R}_b(\omega) \delta\tilde{R}_b^\dagger(\omega) \rangle}{\omega^2 + \tau_E^{-2}} + \frac{\Gamma_Q^2 \langle \delta\tilde{Q}_b(\omega) \delta\tilde{Q}_b^\dagger(\omega) \rangle}{\omega^2 + \tau_E^{-2}} + \frac{\langle \tilde{\xi}_E(\omega) \delta\tilde{\xi}_E^\dagger(\omega) \rangle}{\omega^2 + \tau_E^{-2}}. \quad (19)$$

$\langle \delta\tilde{R}_b(\omega) \delta\tilde{R}_b^\dagger(\omega) \rangle$ can be computed from Eq.(15) as:

$$\langle \delta\tilde{R}_b(\omega) \delta\tilde{R}_b^\dagger(\omega) \rangle = \frac{\langle \tilde{\xi}_R(\omega) \delta\tilde{\xi}_R^\dagger(\omega) \rangle}{\omega^2 + \tau_c^{-2}}. \quad (20)$$

Similarly:

$$\langle \delta\tilde{Q}_b(\omega) \delta\tilde{Q}_b^\dagger(\omega) \rangle = \frac{\langle \tilde{\xi}_Q(\omega) \delta\tilde{\xi}_Q^\dagger(\omega) \rangle}{\omega^2 + \tau_e^{-2}}. \quad (21)$$

From the definition of the Langevin forces (Eq. (11)), it follows:

$$\begin{aligned} \langle \tilde{\xi}_R(\omega) \delta\tilde{\xi}_R^\dagger(\omega) \rangle &= A_R; \\ \langle \tilde{\xi}_Q(\omega) \delta\tilde{\xi}_Q^\dagger(\omega) \rangle &= A_Q; \\ \langle \tilde{\xi}_E(\omega) \delta\tilde{\xi}_E^\dagger(\omega) \rangle &= A_E. \end{aligned}$$

Therefore Eq.(19) becomes:

$$S_E(\omega) = \frac{\Gamma_R^2 A_R}{(\omega^2 + \tau_E^{-2})(\omega^2 + \tau_c^{-2})} + \frac{\Gamma_Q^2 A_Q}{(\omega^2 + \tau_E^{-2})(\omega^2 + \tau_e^{-2})} + \frac{A_E}{\omega^2 + \tau_E^{-2}}. \quad (22)$$

Each Langevin term in the expression above represents a noise source: the first two terms represent the noise in the binding and unbinding of the FGF and ephrin receptors, while the last term represents the noise in the activation of ERK.

The amplitude A_E can be computed following the procedure described in [33] as:

$$A_E = 2V_S \frac{\bar{R}_b^2}{R_b^2 + K_s^2} (E_T - \bar{E}^*). \quad (23)$$

The amplitude A_R can be computed considering that each receptor binding site can be either occupied or empty. The probability that a collection of R receptor binding sites are occupied follows the binomial distribution, therefore the variance of δR_b must be given by:

$$\sigma_{R_b}^2 = \langle (\delta R_b)^2 \rangle = R \bar{n}(1 - \bar{n}). \quad (24)$$

where $\bar{n} = \frac{\bar{R}_b}{R}$ and $m = \frac{\bar{Q}_b}{Q}$ are the fractional occupancy of FGF and ephrin receptors, respectively. At the same time, the variance can be also computed as:

$$\langle (\delta R_b)^2 \rangle = \int \frac{d\omega}{2\pi} S_{R_b}(\omega); \quad (25)$$

where $S_{R_b}(\omega)$ is the power spectral density of the number of bound receptors, that can be computed as $S_{R_b}(\omega) = \langle \delta \tilde{R}_b(\omega) \delta \tilde{R}_b^\dagger(\omega) \rangle$. Comparing the two expressions for the variance one obtains:

$$A_R = \frac{2}{\tau_c} R \bar{n}(1 - \bar{n}). \quad (26)$$

Similarly, A_Q can be computed as:

$$A_Q = \frac{2}{\tau_e} Q \bar{m}(1 - \bar{m}). \quad (27)$$

The total variance of the protein copy number is given by an integral over the spectrum:

$$\langle (\delta E^*)^2 \rangle = \sigma_E^2 = \int \frac{d\omega}{2\pi} S_E(\omega). \quad (28)$$

The noise was computed numerically as a function of c and/or S_1 .

B. Reproduction of the experimental results

Experimentally, ERK activation levels are quantified by immunofluorescence (IF) signals [23]. Thus, to compare the simulation results with experiments we considered that the level of ERK fluorescence (E_f) is a linear function of the number of active ERK molecules (E^*):

$$E_f = A \cdot \frac{E^*}{E_T} + B;$$

where A is the maximal ERK IF signal and B is the background value of the IF signal.

The propagation of the intrinsic noise σ_E to the level of ERK fluorescence is computed as:

$$\Delta E_f = \frac{\partial E_f}{\partial E^*} \sigma_E; \quad (29)$$

where σ_E is computed through the Langevin approach as described in section V A.

Parameter values were obtained by manual fitting to get best agreement with experimental observations. The default values of the parameters are listed in table I.

C. Computation of mutual information in the multiple cell case.

We consider N different cells in contact with FGF and ephrin through the surfaces S_1^i and S_2^i ($i = 1, \dots, N$). In response to the extracellular FGF concentration (indicated as c) different numbers of ERK molecules will be activated in the different cells. Let the number of ERK* molecules in the i -th cell be E_i^* . It is possible to define the mutual information $I(c; \{E_1^*, \dots, E_N^*\})$ transmitted between the input c and the output $\{E_1^*, \dots, E_N^*\}$ as:

$$\begin{aligned} I(c; \{E_1^*, \dots, E_N^*\}) = & - \int P(\{E_1^*, \dots, E_N^*\}) \log_2(P(\{E_1^*, \dots, E_N^*\})) dE_1^* \dots dE_N^* + \\ & + \int P(c) dc \int P(\{E_1^*, \dots, E_N^*\} | c) \log_2(P(\{E_1^*, \dots, E_N^*\} | c)) dE_1^* \dots dE_N^*; \end{aligned} \quad (30)$$

where $P(c)$ is the distribution of the input, $P(\{E_1^*, \dots, E_N^*\})$ is the output distribution and $P(\{E_1^*, \dots, E_N^*\} | c)$ is the conditional distribution of the output given the value of the input. We assume the input distribution $P(c)$ to be a log-normal distribution centered around μ_c with variance σ_c^2 as described in section III B. Since the cells are not interacting the conditional distribution $P(\{E_1^*, \dots, E_N^*\} | c)$ can be written as:

$$P(\{E_1^*, \dots, E_N^*\} | c) = \prod_{i=1}^N P(E_i^* | c). \quad (31)$$

In the absence of more information, we assume that the conditional distributions $P(E_i^* | c)$ are Gaussian:

$$P(E_i^* | c) = \frac{1}{\sqrt{2\pi(\sigma_e^i(c))^2}} e^{-\frac{1}{2} \frac{(E_i^* - \bar{E}_i^*(c))^2}{(\sigma_e^i(c))^2}}; \quad (32)$$

where $\bar{E}_i^*(c)$ is the number of ERK molecules activated in cell i , which is computed solving equations Eq.(1)-(3) at steady-state. $\sigma_e^i(c)$ is the noise in the number of active ERK molecules in the i -th cell which is computed using the Langevin approach as described in section V A.

Finally, the output distribution can be computed di-

rectly from the input and the conditional distribution as:

$$P(\{E_1^*, \dots, E_N^*\}) = \int \prod_{i=1}^N P(E_i^*|c)P(c) dc. \quad (33)$$

All the integrals were evaluated numerically using the composite trapezoidal rule, implemented with the function `numpy.trapz()`.

D. Optimization of information transmission

In the multiple cells case, we considered N cells exposed to FGF and ephrin through the surfaces S_1^i and S_2^i ($i = 1, \dots, N$). In each cell, the surface exposed to ephrin (S_2^i) is computed from the corresponding value of S_1^i using equation Eq.(5). We assume that value of S_1^i in each cell is constrained to be at most equal to $S_{\text{cell}}/2$ (with S_{cell} being the total surface of the cell). The limiting case in which $S_1^i = S_{\text{cell}}/2$ would correspond to the unrealistic condition in which the cell is completely flat. To mimic the presence of the vegetal cells in the embryo, that produce FGF and define a fixed surface in which FGF is present, we consider the presence of an external constraint S_1^{tot} , given by the following equation:

$$\sum_{i=1}^N S_1^i = S_1^{\text{tot}}. \quad (34)$$

We computed the optimal surfaces of the cells $S_1^{*1}, \dots, S_1^{*N}$ that maximize information transmission between the in-

put c and the outputs $\{E_1^*, \dots, E_N^*\}$ and the corresponding maximal amount of information $I^*(c; \{E_1^*, \dots, E_N^*\})$. The constrained optimization was carried out in Python either by brute-force (in the two-cells case) or by using the Constrained Optimization BY Linear Approximation (COBYLA) method (in the three and four-cells cases) which is an iterative method for derivative-free constrained optimization.

E. Experimental methods

All the experimental results are taken from our previous work [23].

ACKNOWLEDGMENTS

We thank very warmly Clare Hudson and Hiroyoshi Yasuo for their thoughtful comments about the manuscript and for answering many of our questions about ascidians. RB is supported by a FRIA fellowship. GD is Research Director at the Belgian "Fonds National pour la Recherche Scientifique" (FRS-FNRS) and acknowledges financial support from the ARC project "Noise sensitivity of gene regulatory networks underlying cell fate specification" financed by the Université libre de Bruxelles (ULB). AMW is supported by ANR Distant and CZI Biohub Theory Initiative. The funders had no role in study design, data collection and analysis, decision to publish, or preparation of the manuscript. The resources and services used in this work were provided by the VSC (Flemish Supercomputer Center), funded by the Research Foundation - Flanders (FWO) and the Flemish Government.

-
- [1] S. Laughlin, A Simple Coding Procedure Enhances a Neuron's Information Capacity, *Zeitschrift für Naturforschung C* **36**, 910 (1981).
- [2] G. Tkačik, C. G. Callan, and W. Bialek, Information flow and optimization in transcriptional regulation, *Proceedings of the National Academy of Sciences* **105**, 12265 (2008).
- [3] M. D. Petkova, G. Tkačik, W. Bialek, E. F. Wieschaus, and T. Gregor, Optimal Decoding of Cellular Identities in a Genetic Network, *Cell* **176**, 844 (2019).
- [4] D. B. Brückner and G. Tkačik, Information content and optimization of self-organized developmental systems (2023), arXiv:2312.05895 [cond-mat, physics:nlin, physics:physics, q-bio].
- [5] G. Tkacik, A. M. Walczak, and W. Bialek, Optimizing information flow in small genetic networks. I, *Physical Review E* **80**, 031920 (2009), arXiv:0903.4491 [q-bio].
- [6] G. Tkačik and A. M. Walczak, Information transmission in genetic regulatory networks: A review, *Journal of Physics. Condensed Matter: An Institute of Physics Journal* **23**, 153102 (2011).
- [7] G. Fernandes, H. Tran, M. Andrieu, Y. Diaw, C. Perez Romero, C. Fradin, M. Coppey, A. M. Walczak, and N. Dostatni, Synthetic reconstruction of the hunchback promoter specifies the role of Bicoid, *Zelda and Hunchback in the dynamics of its transcription*, *eLife* **11**, e74509 (2022).
- [8] G. Tkačik and T. Gregor, The many bits of positional information, *Development* **148**, dev176065 (2021).
- [9] C. J. Miller and L. A. Davidson, The interplay between cell signalling and mechanics in developmental processes, *Nature Reviews Genetics* **14**, 733 (2013).
- [10] S. Liu, P. Lemaire, E. Munro, and M. Mani, A mechanical atlas for Ascidian gastrulation (2022).
- [11] S. Ichbiah, F. Delbary, A. McDougall, R. Dumollard, and H. Turlier, Embryo mechanics cartography: Inference of 3D force atlases from fluorescence microscopy, *Nature Methods* **20**, 1989 (2023).
- [12] R. Dumollard, N. Minc, G. Salez, S. B. Aicha, F. Bekkouche, C. Hebras, L. Besnardeau, and A. McDougall, The invariant cleavage pattern displayed by ascidian embryos depends on spindle positioning along the

- cell's longest axis in the apical plane and relies on asynchronous cell divisions, *eLife* **6**, e19290 (2017).
- [13] C. H. Waddington, CANALIZATION OF DEVELOPMENT AND THE INHERITANCE OF ACQUIRED CHARACTERS, *Nature* **150**, 563 (1942).
- [14] P. Lemaire, Evolutionary crossroads in developmental biology: The tunicates, *Development* **138**, 2143 (2011).
- [15] M. Brozovic, C. Dantec, J. Dardaillon, D. Dauga, E. Faure, M. Gineste, A. Louis, M. Naville, K. R. Nitta, J. Piette, W. Reeves, C. Scornavacca, P. Simion, R. Vincentelli, M. Bellec, S. B. Aicha, M. Fagotto, M. Guérout-Bellone, M. Haeussler, E. Jacox, E. K. Lowe, M. Mendez, A. Roberge, A. Stolfi, R. Yokomori, C. T. Brown, C. Cambillau, L. Christiaen, F. Delsuc, E. Douzery, R. Dumollard, T. Kusakabe, K. Nakai, H. Nishida, Y. Satou, B. Swalla, M. Veeman, J.-N. Volff, and P. Lemaire, ANISEED 2017: Extending the integrated ascidian database to the exploration and evolutionary comparison of genome-scale datasets, *Nucleic Acids Research* **46**, D718 (2018).
- [16] K. S. Imai, M. Levine, N. Satoh, and Y. Satou, Regulatory Blueprint for a Chordate Embryo, *Science* **312**, 1183 (2006).
- [17] Y. Satou and K. S. Imai, Gene regulatory systems that control gene expression in the *Ciona* embryo, *Proceedings of the Japan Academy, Series B* **91**, 33 (2015).
- [18] S. Sharma, W. Wang, and A. Stolfi, Single-cell transcriptome profiling of the *Ciona* larval brain, *Developmental Biology* **448**, 226 (2019).
- [19] L. Guignard, U.-M. Fiúza, B. Leggio, J. Laussu, E. Faure, G. Michelin, K. Biasuz, L. Hufnagel, G. Malandain, C. Godin, and P. Lemaire, Contact area-dependent cell communication and the morphological invariance of ascidian embryogenesis, *Science (New York, N.Y.)* **369**, eaar5663 (2020).
- [20] K. M. Winkley, W. M. Reeves, and M. T. Veeman, Single-cell analysis of cell fate bifurcation in the chordate *Ciona*, *BMC Biology* **19**, 180 (2021).
- [21] J. L. Christian, Morphogen gradients in development: From form to function, *Wiley Interdisciplinary Reviews. Developmental Biology* **1**, 3 (2012).
- [22] R. Bettoni, C. Hudson, G. Williaume, C. Sirour, H. Yasuo, S. de Buyl, and G. Dupont, Model of neural induction in the ascidian embryo, *PLoS computational biology* **19**, e1010335 (2023).
- [23] G. Williaume, S. de Buyl, C. Sirour, N. Haupaix, R. Bettoni, K. S. Imai, Y. Satou, G. Dupont, C. Hudson, and H. Yasuo, Cell geometry, signal dampening, and a bimodal transcriptional response underlie the spatial precision of an ERK-mediated embryonic induction, *Developmental Cell* **56**, 2966 (2021).
- [24] P. Lemaire, V. Bertrand, and C. Hudson, Early Steps in the Formation of Neural Tissue in Ascidian Embryos, *Developmental Biology* **252**, 151 (2002).
- [25] B. Liu and Y. Satou, The genetic program to specify ectodermal cells in ascidian embryos, *Development, Growth & Differentiation* **62**, 301 (2020).
- [26] C. Hudson and P. Lemaire, Induction of anterior neural fates in the ascidian *Ciona intestinalis*, *Mechanisms of Development* **100**, 189 (2001).
- [27] H. Lavoie, J. Gagnon, and M. Therrien, ERK signalling: A master regulator of cell behaviour, life and fate, *Nature Reviews Molecular Cell Biology* **21**, 607 (2020).
- [28] C. E. Shannon, A Mathematical Theory of Communication, *Bell System Technical Journal* **27**, 379 (1948).
- [29] P. Lemaire, Unfolding a chordate developmental program, one cell at a time: Invariant cell lineages, short-range inductions and evolutionary plasticity in ascidians, *Developmental Biology* **332**, 48 (2009).
- [30] K. Biasuz, *Analyse quantitative et systématique de la dynamique spatio-temporelle de l'activité de la voie de signalisation ERK au cours de l'embryogenèse des ascidies*, Theses, Université de Montpellier (2022).
- [31] R. Blahut, Computation of channel capacity and rate-distortion functions, *IEEE Transactions on Information Theory* **18**, 460 (1972).
- [32] A. Stolfi, E. K. Lowe, C. Racioppi, F. Ristoratore, C. T. Brown, B. J. Swalla, and L. Christiaen, Divergent mechanisms regulate conserved cardiopharyngeal development and gene expression in distantly related ascidians, *eLife* **3**, e03728 (2014).
- [33] D. T. Gillespie, The chemical Langevin equation, *The Journal of Chemical Physics* **113**, 297 (2000).

Appendix: Optimizing information between S_1 and E^*

In this work we maximized the information transmitted between the extracellular [FGF] and the number of active ERK* molecules to find the optimal geometrical configuration of the cell (i.e., the optimal value of S_1). The same problem of optimizing information transmission can be tackled considering the surface S_1 as the input of the signaling cascade. In this case we can compute the information $I(S_1, E^*)$, and find the optimal distribution of the input $P^*(S_1)$. We will describe below the computation in the case of a single cell. To perform the optimization we follow the procedure described in [2, 5, 6]. When considering multiple cells the analytical approach becomes challenging and numerical techniques must be used. We leave this more complicated problem for future studies.

The information transmitted between S_1 and E^* can be written as:

$$I(S_1; E^*) = - \int P(E^*) \log_2(P(E^*)) dE^* + \int P(S_1) dS_1 \int P(E^*|S_1) \log_2(P(E^*|S_1)) dE^*. \quad (\text{A.1})$$

We assume that the conditional distribution $P(E^*|S_1)$ to be Gaussian:

$$\mathcal{G}(E^*, \bar{E}^*(S_1), \sigma_e^2(S_1)); \quad (\text{A.2})$$

where $\bar{E}^*(S_1)$ and $\sigma_e^2(S_1)$ are computed as described in section III A and V A.

The integral $\int P(E^*|S_1) \log_2(P(E^*|S_1)) dE^*$ is simply (minus) the entropy of the Gaussian distribution, which can be computed as $\log_2(\sqrt{2\pi e} \sigma_e(S_1))$.

The output distribution can be computed as:

$$P(E^*) = \int P(E^*|S_1) P(S_1) dS_1. \quad (\text{A.3})$$

In the small noise limit, we can approximate $P(E^*|S_1)$ with a delta function:

$$P(E^*|S_1) \simeq \delta(E^* - \bar{E}^*(S_1)). \quad (\text{A.4})$$

As a result, we can rewrite the output distribution $P(E^*)$ in terms of the input distribution $P(S_1)$ as:

$$P(E^*) \simeq P(S_1) \left| \frac{d\bar{E}^*}{dS_1} \right|. \quad (\text{A.5})$$

Information therefore becomes:

$$I(S_1; E^*) = \int P(S_1) \log_2 \left(\frac{|d\bar{E}^*/dS_1|}{\sqrt{2\pi e} \sigma_e P(S_1)} \right) dS_1. \quad (\text{A.6})$$

1. In the absence of external constraints

To maximize information we write the Lagrangian:

$$\mathcal{L}[P(S_1)] = I(S_1; E^*) - \Lambda \left(\int P(S_1) dS_1 - 1 \right); \quad (\text{A.7})$$

where Λ is a Lagrange multiplier that will enforce the normalization of the input distribution $P(S_1)$. The optimal input distribution $P^*(S_1)$ must satisfy:

$$\frac{\partial \mathcal{L}[P(S_1)]}{\partial P(S_1)} = 0. \quad (\text{A.8})$$

As a result, the optimal distribution is given by:

$$P^*(S_1) = \frac{1}{Z} \left| \frac{dE^*}{dS_1} \right| \frac{1}{\sigma_e(S_1)}, \quad (\text{A.9})$$

where the normalization constant Z is:

$$Z = \int \left| \frac{dE^*}{dS_1} \right| \frac{1}{\sigma_e(S_1)} dS_1.$$

The maximal amount of information is obtained inserting the expression for $P^*(S_1)$ in Eq.(A.6):

$$I^*(S_1; E^*) = \log_2(Z). \quad (\text{A.10})$$

The optimal input distribution (shown in red) is compared with the input-output curve $E^*(S_1)$ (shown in orange) in Fig. 5.

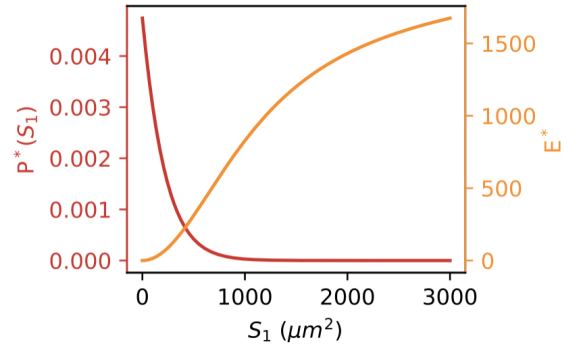


FIG. 5. Optimal input distribution $P^*(S_1)$ (in red). In orange is shown the input-output relation $E^*(S_1)$. The plot is obtained assuming $S_{cell} = 6000 \mu\text{m}^2$, $c = 40$. The value of S_1 is constrained to be at most equal to $S_{cell}/2$.

2. In the presence of the constraint $\langle S_1 \rangle = S_1^{tot}$

We now consider the presence of an external constraint that fixes the average area of the cell surface in contact with FGF: $\langle S_1 \rangle = S_1^{tot}$. In the presence of the constraint the Lagrangian becomes:

$$\mathcal{L}[P(S_1)] = I(S_1; E^*) - \Lambda \left(\int P(S_1) dS_1 - 1 \right) - \Gamma \left(\int S_1 P(S_1) dS_1 - S_1^{tot} \right); \quad (\text{A.11})$$

where Γ is the Lagrange multiplier that fixes the average surface of the cell $\langle S_1 \rangle = S_1^{tot}$. The optimal input distribution in this case becomes:

$$P^*(S_1) = \frac{1}{Z} \left| \frac{dE^*}{dS_1} \right| \frac{1}{\sigma_e(S_1)} e^{-\Gamma S_1}, \quad (\text{A.12})$$

with:

$$Z = \int \left| \frac{dE^*}{dS_1} \right| \frac{1}{\sigma_e(S_1)} e^{-\Gamma S_1} dS_1.$$

The maximal information is:

$$I^*(S_1; E^*) = \log_2(Z) + \Gamma S_1^{tot}. \quad (\text{A.13})$$

The information transmitted as a function of S_1^{tot} is shown in Fig. 6. The curve has a maximum for intermediate values of $\langle S_1 \rangle \simeq 1340 \mu m^2$, qualitatively in agreement with the results obtained for the single cell case in section III B.

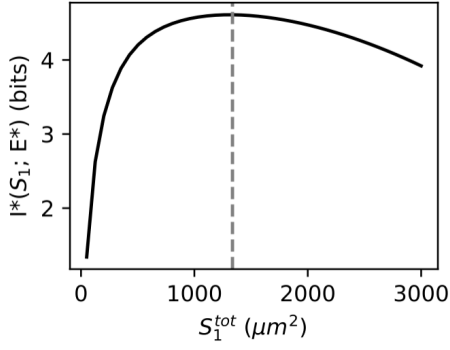


FIG. 6. Maximal information $I^*(S_1; E^*)$ transmitted for increasing values of S_1^{tot} . The vertical gray line highlights the position of the maximum (which occurs at $\langle S_1 \rangle \simeq 1340 \mu m^2$). The plot is obtained assuming $S_{cell} = 6000 \mu m^2$, $c = 40$. The value of $\langle S_1 \rangle = S_1^{tot}$ is constrained to be at most equal to $S_{cell}/2$.

SUPPLEMENTARY MATERIAL

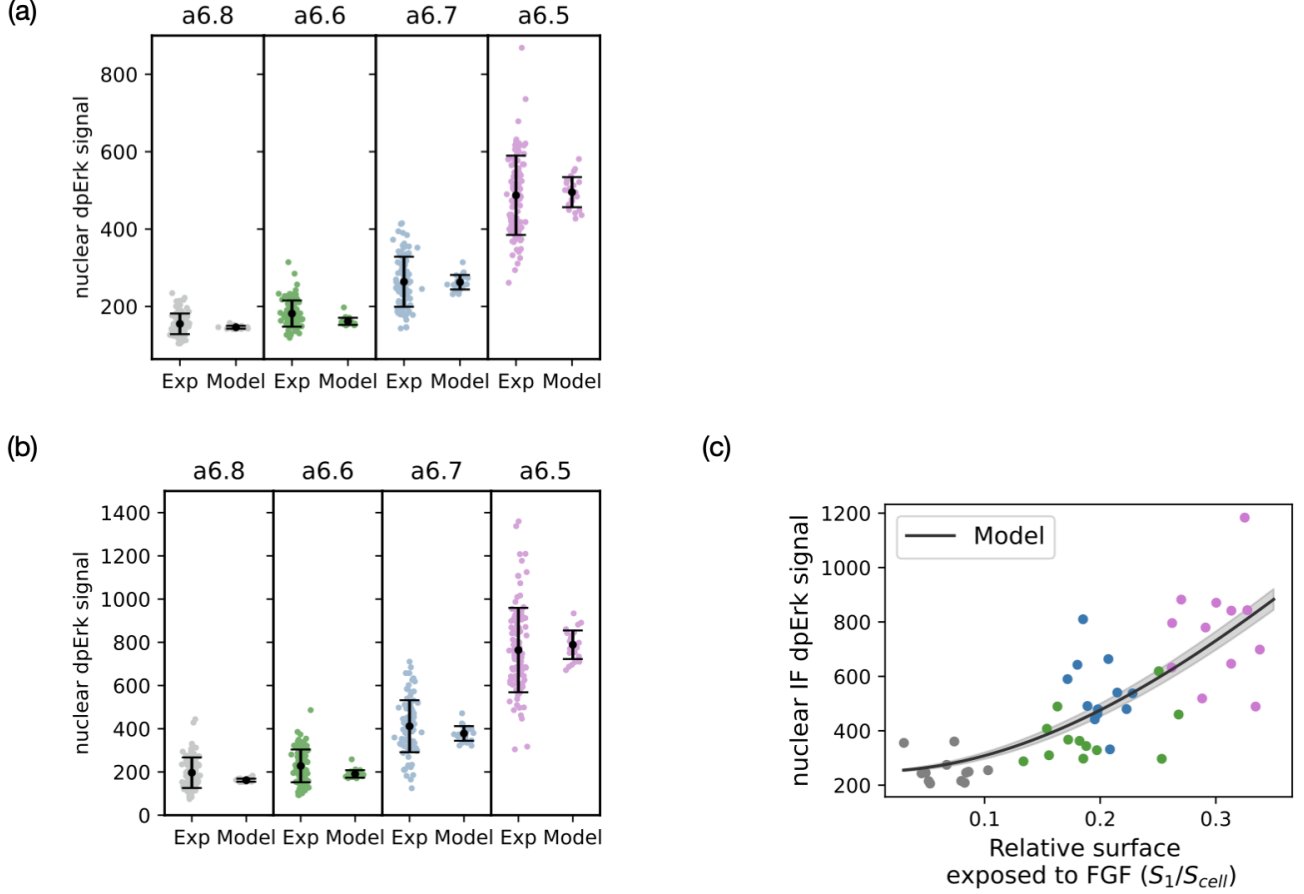


FIG. S1. (a) Nuclear dpERK immunofluorescence (IF) signals in the a6.5, a6.6, a6.7 and a6.8 cell types as measured in IF experiments in wild type embryos (left) and computed with the model (right). Each point represents a single cell and modeling results are computed using the measured values of S_1 . Means and standard deviations are shown in black. The parameter values used to reproduce the experimental data are listed in table I. $A = 5000$, $B = 140$. (b) Nuclear dpERK immunofluorescence (IF) signals in the a6.5, a6.6, a6.7 and a6.8 cell types as measured in IF experiments in embryos in which the ephrin pathway was inhibited (left) and computed with the model (right). Each point represents a single cell and modeling results are computed using the measured values of S_1 . Means and standard deviations are shown in black. The parameter values used to reproduce the experimental data are listed in table I. $A = 8000$, $B = 150$. To mimic the absence of ephrin, we imposed $e = 10^{-5}$. (c) Experimental data in the absence of ephrin. The plot shows the nuclear dpERK immunofluorescence (IF) signals measured experimentally in individual a-line cells as a function of the relative area of cell surface contact with FGF-expressing cells (S_1/S_{cell}). Experimental data obtained in the different cell types are shown with dots of different colors: a6.8 cells are shown in gray, a6.6 cells in green, a6.7 cells in blue, and a6.5 cells in magenta. The experimental data obtained in embryos in which the ephrin pathway is inhibited are compared with the model predictions (shown with a black line). The shaded region represents the noise in the level of ERK* fluorescence predicted by the model using the Langevin approach. The model predictions are obtained as described in section III A, V A and V B. The parameter values used to reproduce the experimental data are listed in table I. $A = 10000$, $B = 250$. To mimic the absence of ephrin, we imposed $e = 10^{-5}$.

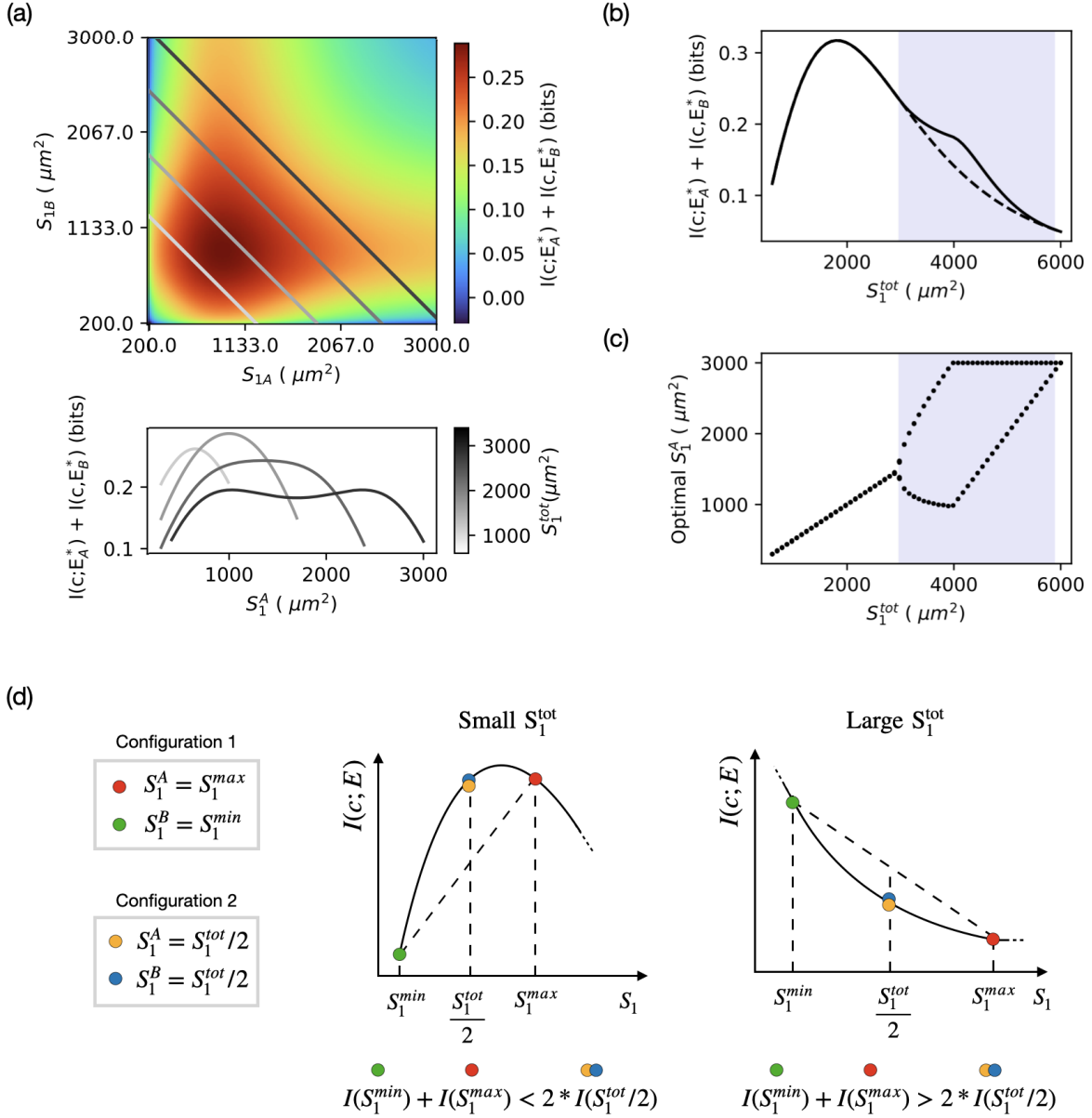


FIG. S2. (a) Independent cell case. The heat map represents the information transmitted assuming the two cells are independent $I = I(c; E_A) + I(c; E_B)$ as a function of the area of cell surfaces exposed to FGF (S_1^A and S_1^B). The presence of the constraint restricts the possible values of S_1^A and S_1^B to straight lines defined by $S_1^B = S_1^{\text{tot}} - S_1^A$. The straight lines colored with different shades of gray represent the accessible values of S_1^A and S_1^B for the values of S_1^{tot} used in the plot below. The plot below represents $I = I(c; E_A) + I(c; E_B)$ as a function of S_1^A for different values of the constraint S_1^{tot} (see colorbar). (b) Maximal information (solid line, obtained when the two cells expose the optimal surface areas to FGF) and the information transmitted when the two cells have the same surface areas exposed to FGF (dashed line) as a function of S_1^{tot} . (c) Optimal values of S_1^A as a function of S_1^{tot} . The purple background highlights the regions of the plots where it is maximally informative for the two cells to expose different surface areas to FGF. Panels (a), (b) and (c) are obtained assuming $\mu_c = 40$, $\sigma_c = 1$, $S_{\text{cell}}^A = S_{\text{cell}}^B = 6000 \mu\text{m}^2$. (d) Scheme illustrating why the optimal geometrical configuration of the cells vary with S_1^{tot} . We compare two geometrical configurations of the cells: configuration 1 in which $S_1^A = S_1^{\text{max}}$ and $S_1^B = S_1^{\text{min}}$, and configuration 2 in which $S_1^A = S_1^B = S_1^{\text{tot}}/2$. S_1^{min} and S_1^{max} are the maximal and minimal possible values for S_1 (fixed by the values of S_{cell} and S_1^{tot}). At low values of S_1^{tot} the part of the curve accessible is concave. In this condition, it is easy to see that the configuration of the cells that maximizes information transmission is configuration 2 ($S_1^A = S_1^B = S_1^{\text{tot}}/2$). At large values of S_1^{tot} , the part of the curve that is accessible is convex. In this condition, the configuration that maximizes information transmission is configuration 1 ($S_1^A \neq S_1^B$).

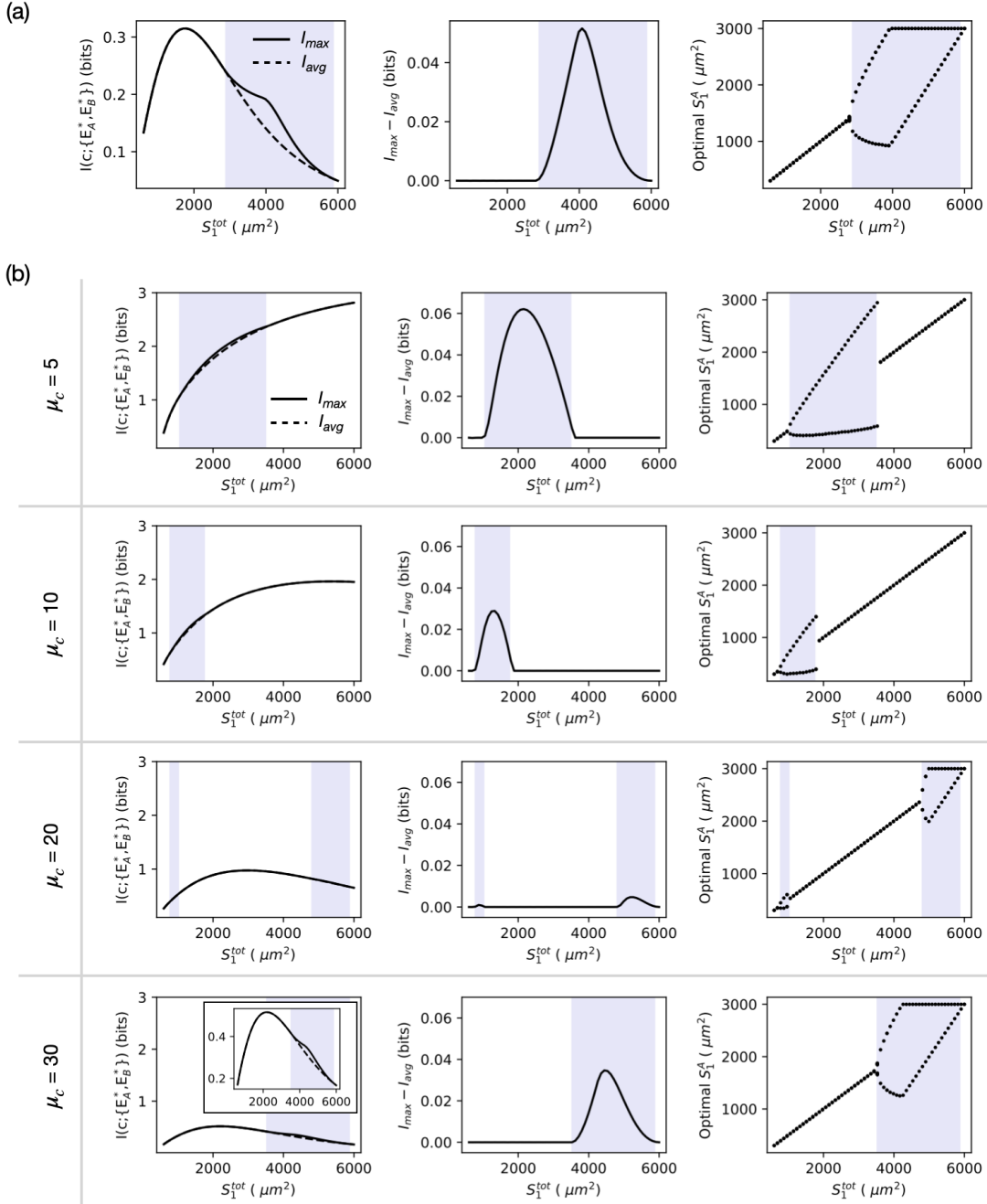


FIG. S3. (a) Information transmission in the absence of ephrin. The plot on the left shows the maximal information (I_{\max}) transmitted between c and $\{E_A^*, E_B^*\}$ (solid line, obtained when the cells expose the optimal surfaces to FGF) and the information transmitted when the two cells expose the same surface to FGF (I_{avg} , dashed line) as a function of S_1^{tot} . The plot in the middle shows the difference between I_{\max} and I_{avg} as a function of S_1^{tot} . The plot on the right shows the values of the optimal surface S_1^{A*} as a function of S_1^{tot} . The purple background highlights the regions of the plots where it is better, in order to maximize information transmission, for the two cells to break the symmetry and expose different surfaces to FGF. These plots are obtained assuming that the input distribution $P(c)$ is centered around $\mu_c = 40$ and that the two cells have the same total surface $S_{\text{cell}}^A = S_{\text{cell}}^B = 6000 \mu\text{m}^2$. To model the absence of ephrin we used $e = 10^{-5}$. (b) Influence of the position μ_c of the input distribution on information transmission. The plots in the first column show the maximal information (I_{\max}) transmitted between c and $\{E_A^*, E_B^*\}$ (solid line, obtained when the cells expose the optimal surfaces to FGF) and the information transmitted when the two cells expose the same surface to FGF (I_{avg} , dashed line) as a function of S_1^{tot} . The plots in the second column show the difference between I_{\max} and I_{avg} as a function of S_1^{tot} . The plots in the third column show the values of the optimal surface S_1^{A*} as a function of S_1^{tot} . The purple background highlights the regions of the plots where it is better, in order to maximize information transmission, for the two cells to break the symmetry and expose different surfaces to FGF. These plots are obtained assuming that the two cells have the same total surface $S_{\text{cell}}^A = S_{\text{cell}}^B = 6000 \mu\text{m}^2$.

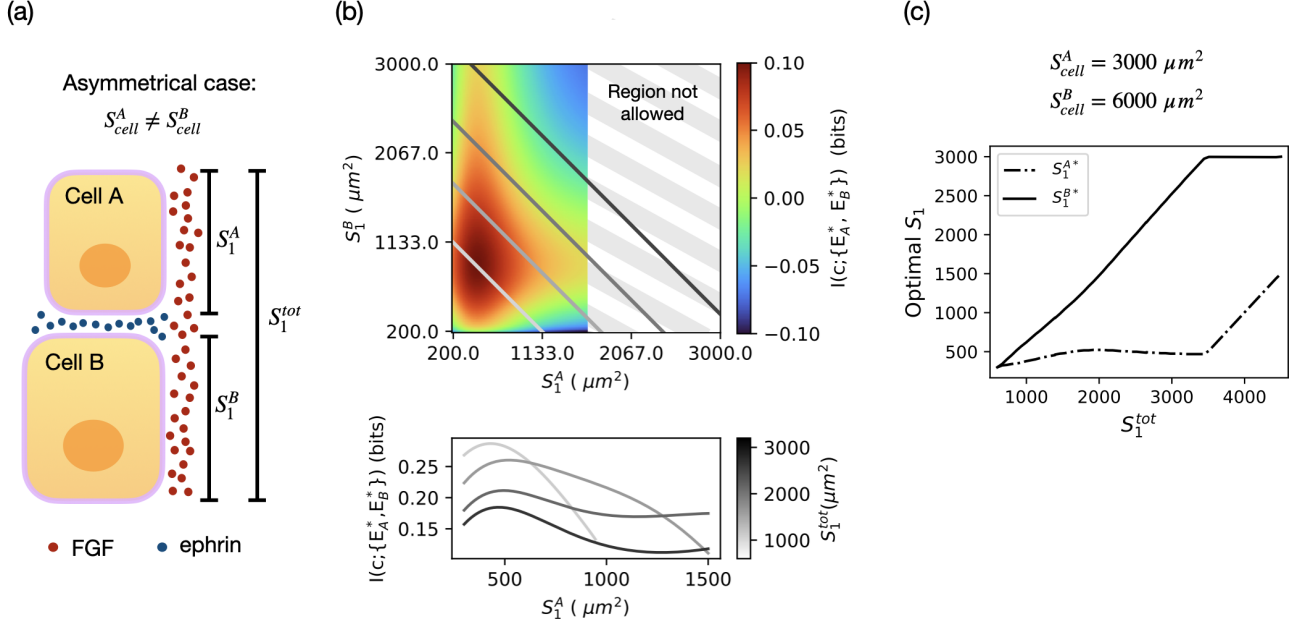


FIG. S4. Two-cells: asymmetrical case. (a) In the asymmetrical case we consider that the two cells have different cell surface areas ($S_{cell}^A \neq S_{cell}^B$). S_1^A and S_1^B are the surface areas of the cells exposed to FGF. S_2^A and S_2^B (not shown in the cartoon) are the surface areas of the cells exposed to ephrin. In each cell, $S_2^{A,B}$ is computed from the corresponding value of $S_1^{A,B}$ using equation Eq.(5). The value of S_1 in each cell is constrained to be at most equal to $S_{cell}/2$, with S_{cell} being the total surface area of the cell. S_1^{tot} represents the total surface area where FGF is present. The presence of the constraint implies that $S_1^A + S_1^B = S_1^{tot}$. (b) The heatmap represents the information transmitted between the FGF input c and the ERK output $\{E_A^*, E_B^*\}$ as a function of the area of cell surfaces exposed to FGF (S_1^A and S_1^B). The presence of the constraint restricts the possible values of S_1^A and S_1^B to straight lines defined by $S_1^B = S_1^{tot} - S_1^A$. The straight lines colored with different shades of gray represent the accessible values of S_1^A and S_1^B for the values of S_1^{tot} used in the plot below. The plot below represents $I(c; \{E_A^*, E_B^*\})$ as a function of S_1^A for different values of the constraint S_1^{tot} (see colorbar). (c) The plot shows the optimal values of the surfaces exposed to FGF (S_1^{A*} with a dashed line and S_1^{B*} with a solid line) as a function of the value of the constraint S_1^{tot} . The optimal values are obtained maximizing information transmission assuming $\mu_c = 40$, $S_{cell}^A = 3000 \mu m^2$, $S_{cell}^B = 6000 \mu m^2$.